HYDROGRAPHY OF THE RUSSIAN RIVER ESTUARY

SUMMER-FALL 2009

WITH SPECIAL ATTENTION ON A FIVE-WEEK CLOSURE EVENT

John Largier[1] & Dane Behrens[2]

Bodega Marine Laboratory

University of California Davis

1. Also in Department of Environmental Science and Policy

2. Also in Department of Civil and Environmental Engineering

Acknowledgements: This report was prepared for and funded by the Sonoma County Water Agency. We thank Chris Delaney (SCWA), Matt Brennan (PWA), Fabian Bombardelli (UCD) and Jeff Church (SCWA) for valuable discussions. We thank Jeff Church at SCWA as well as Matt Robart, David Dann, Megan Sheridan, and other colleagues at BML/UCD for their assistance in the fieldwork – including summer REU student Aaron Tamminga. Warm thanks go to Elinor Twohy, whose hospitality was a critical help in the long days of fieldwork.

Executive Summary

Circulation, stratification and water properties were monitored during late summer 2009 in the Russian River estuary– a dry year in which river flow was lower level than normal. Attention is directed at conditions in a month-long closure event in September-October. A dense lower layer of high-salinity water was trapped in the estuary when the mouth closed, with stability increasing over time as well as an expansion of stable stratification as saline waters intruded into the inner estuary. Within a week of strong stratification being established, the near-bottom waters became hypoxic. At mid-depth penetration of light led to photosynthesis and a stable layer in which oxygen levels were high during the day. At similar depths, thermal radiation was also trapped and water temperatures were greatest. The thin surface layer was well mixed and in equilibrium with the atmosphere in terms of both dissolved oxygen and temperature. Stratification and deep-water hypoxia persisted until tidal action returned with opening of the mouth in October.

This report is preceded by a data report (Behrens & Largier 2010), in which all field data are plotted and details are provided on instrument deployments. In this report, core sections address (i) water budget and seepage analysis, (ii) tidal and diurnal currents, (iii) hydrographic structure – salinity, temperature, dissolved oxygen, (iv) stratification and water column stability, (v) salt and dissolved oxygen budgets.

Central to this study and the value of the Russian River estuary as habitat for juvenile salmon is the strong stratification that develops due to trapping of a salt layer in the estuary when the mouth closes. The salt-stratified closed estuary is non-tidal and a wind-driven diurnal seiche takes on particular importance in the horizontal redistribution of salt as well as in raising the possibility of vertical mixing and eventual breakdown of the stratification. Breakdown of stratification appears essential for re-oxygenating the hypoxic bottom waters and reducing mid-depth temperatures. A significant apparent loss of estuary water through the sand barrier (~60cfs) is important in flushing the surface layer (residence time order 10 days), but it plays only a minor role in reducing the salinity of the lower layer within 1-2 km of the barrier beach.

The most significant advances in future understanding in support of improved management of the estuary are likely to come from (i) linking water property distributions to salmon habitat value and extent, (ii) assessment of the extent of hypoxia immediately following breaching after a long closure, (iii) assessment of turbulence, vertical mixing and the potential for breakdown of stratification, (iv) a fuller quantification and understanding of the diurnal wind-driven seiche, (v) a fuller quantification and understanding of seepage losses through the sand barrier, and (vi) a fuller quantification and understanding of berm overflows and wave overwash.

This page intentionally blank.

Table of Contents

Acronyms & Terminology

ADCP	acoustic doppler current profiler
anoxic	zero dissolved oxygen
barotropic	pressure gradient due to sloping water level is uniform with depth
baroclinic	pressure gradient due to gradient in density increases with depth
BML	Bodega Marine Laboratory, University of California Davis
BOD	biochemical oxygen demand
BOON	Bodega Ocean Observing Node (http://www.bml.ucdavis.edu/boon/)
CDIP	Coastal Data Information Program (http://cdip.ucsd.edu/)
CTD	conductivity-temperature-depth profiling instrument
DO	dissolved oxygen
DWR	California Department of Water Resources
halocline	level at which salinity changes suddenly with depth
hypoxic	very low level of dissolved oxygen (typically below 2mg/l)
hypsometric curve	curve that shows plan area of estuary at different elevations (when integrated, curve gives estuary volume below that elevation)
isothermal	no spatial difference in temperature
isopycnal	no spatial difference in density; or line of equal density
NDBC	National Data Buoy Center (http://www.ndbc.noaa.gov/)
NMFS	National Marine Fisheries Service (http://www.nmfs.noaa.gov/)
PAR	photosynthetically active radiation
ppt	parts per thousand (by mass)
psu	practical salinity units
PWA	Philip Williams & Associates (http://www.pwa-ltd.com/)
pycnocline	level at which density changes suddenly
SBE	SeaBird Electronics (http://www.seabird.com/)
SCWA	Sonoma County Water Agency (http://www.scwa.ca.gov/)
seiche	rhythmic swash of water in a basin, from one end to the other, and back
thermocline	level at which temperature changes suddenly

1. Introduction

The Russian River Biological Opinion written by the National Marine Fisheries Service (NMFS 2008) requires the Sonoma County Water Agency (SCWA) to manage the Russian River estuary in such a way as to maintain a closed mouth following natural closure during the summer management period of 15 May through 15 October. It is expected that this closed lagoon state was typical in late summer and fall prior to human perturbations of the system and that this closed lagoon state will provide improved habitat for the rearing of juvenile steelhead in the estuary (and possibly also coho). However, long-duration closures of the Russian River estuary have not been observed recently and it is unclear how stratification and water residence will play out in terms of the distribution of water properties (specifically salinity, temperature, velocity, and dissolved oxygen). Water properties are key determinants of juvenile steelhead habitat, and they are important in their relation to water quality conditions conducive to ecosystem health and human “beneficial uses”.

Bodega Marine Laboratory (BML) at the University of California Davis was contracted by the SCWA to conduct a study of the estuary that provides a view of circulation, stratification, salinity, and residence during the summer and fall of 2009. The aim was to provide SCWA with a basis for designing a more complete hydrological analysis by identifying phenomena and processes that are critical to future management of the estuary and the multiple human and ecosystem uses of this environment. Data were collected as a basis for (i) assessment of the hydrological condition of the estuary during the 2009 dry season, (ii) future analyses that will provide understanding of how river flow and mouth state control estuary hydrology and through that water-column habitat in the estuary, and (iii) validation and inputs for future numerical modeling of the estuary.

The Russian River estuary is a bar-built, drowned-river-valley estuary. Although this type of estuary is common – indeed typical – in central and northern California, the characteristic hydrological patterns and underlying hydrodynamic processes are not well documented nor understood. In this study, it was necessary to obtain primary field data and to conduct data analyses in order to obtain a preliminary understanding of this system and thus to allow discussion of possible future conditions.

This report is a summary of results from the field program in the Russian River estuary during the summer and fall of 2009, during which river flows were lower than normal. This report is preceded by a data report (Behrens & Largier 2010), in which all field data are described and graphically presented.

2. Field Data

The study area extended from the mouth of the Russian River estuary to Austin Creek. Fieldwork consisted of four components, described below (Figure 2.1):
(1) Time-series of pressure/temperature measurements at 4 locations, for monitoring water surface elevation.
(2) Vertical profiles of conductivity-temperature-depth (CTD) at fixed stations along the axis of estuary.
(3) Time-series of vertical profiles of currents – acoustic doppler current profiler (ADCP).
(4) Time-series of near-bottom salinity/temperature measurements at 3 locations.

These data are described in detail and all data are plotted in the companion data report (Behrens & Largier 2010). These data are combined with sonde data from SCWA and with data on waves, river flow, wind and bathymetry obtained from other sources (see below) to provide a description of hydrographic conditions and an understanding of hydrodynamic controls in the Russian River estuary during late summer and fall 2009.

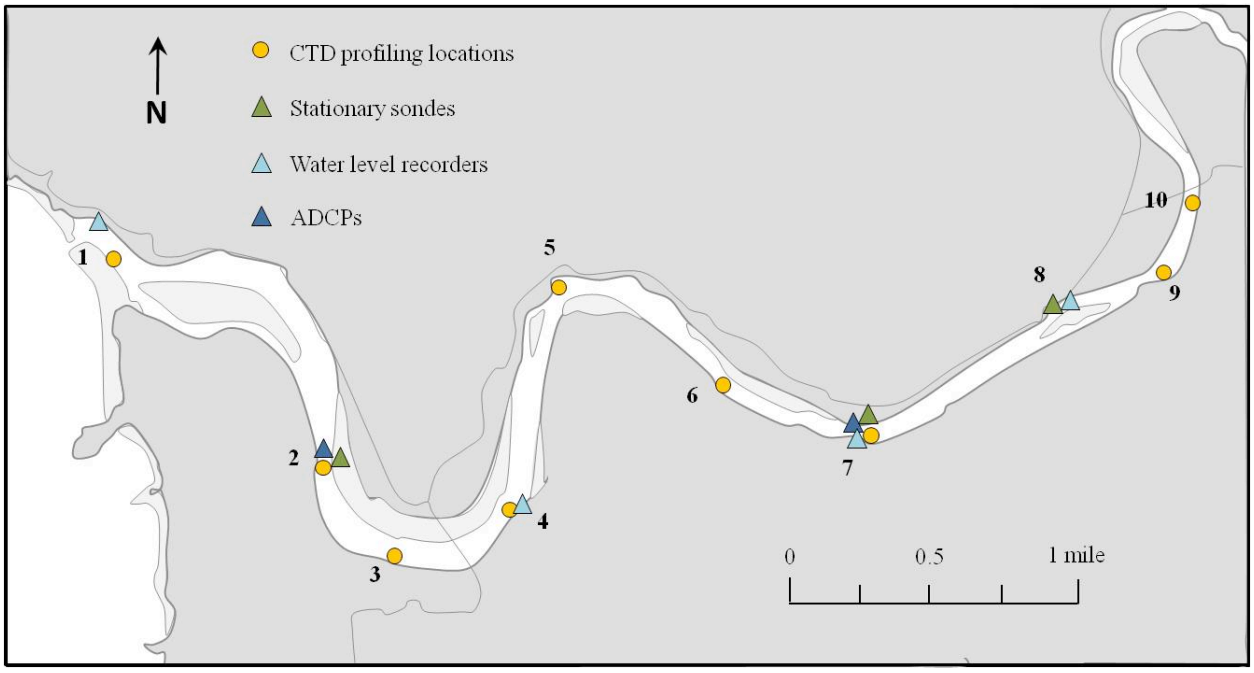

Figure 2.1. *Measurement locations: 1 - Mouth, 2 - Paddy's Rock, 3 - Bridgehaven, 4 - Willow Creek, 5 - Sheephouse Creek, 6- Osprey Rookery, 7 - Heron Rookery, 8 - Freezeout Island, 9 - Freezeout Creek and 10 - Moscow Bridge.*

The study was conducted from June through December 2009. The estuary mouth remained open following a brief closure period in late June and tidal fluctuations in the estuary reflected spring-neap cycles and the degree of tidal constriction at the mouth. An extended mouth closure event started on 7 September, following several days of muted tides (Figure 2.2). The mouth remained closed until 6 October. It remained open for about a week before closing again in mid-October. The September-October event provided an opportunity to study the conditions during a prolonged closure event at high temporal resolution.

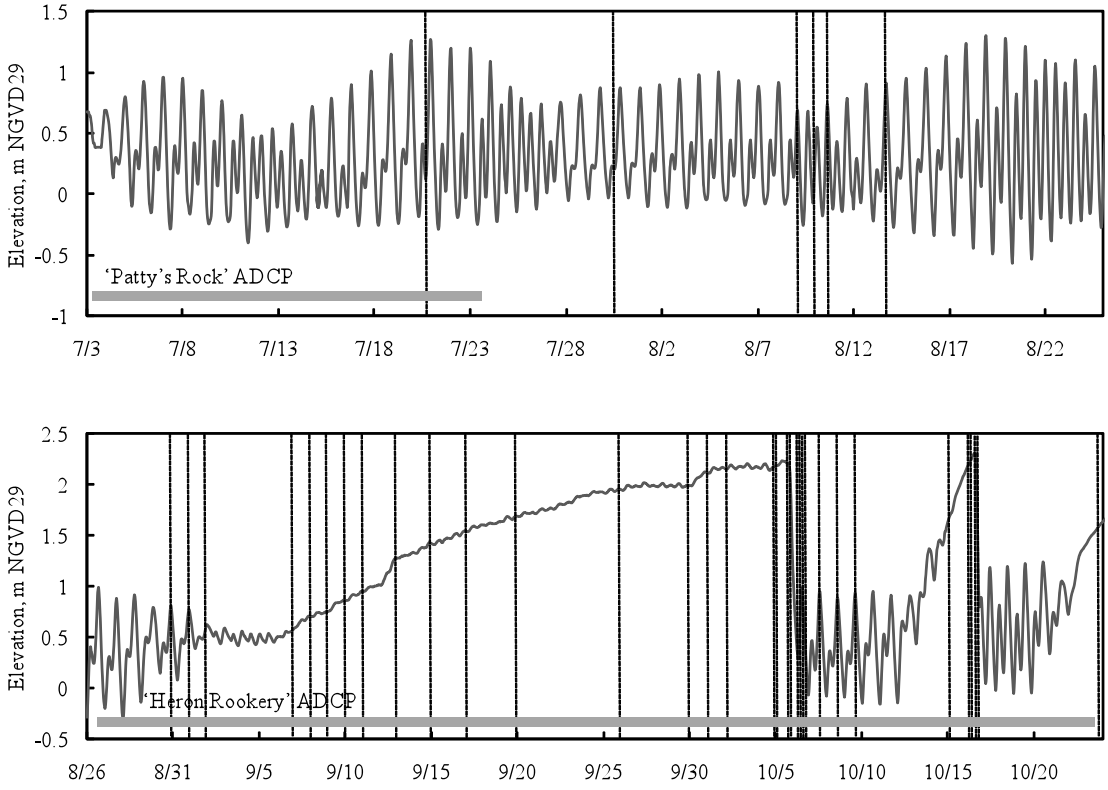

Figure 2.2 *Water level record during study period, providing a study timeline and indicating periods of ADCP deployment (horizontal grey bars) and times that CTD profiles were taken (vertical dashed lines).*

2.1 – Time-series of water level elevations

Four HOBO water level loggers were deployed in August, at locations shown in Figure 2.1. The loggers record temperature and pressure at two-minute intervals. Atmospheric pressure (measured at BML) was subtracted from the measured pressure to obtain

gage pressure (i.e., pressure due to the weight of the overlying water). Gage pressure and temperature were used in conjunction with surface salinity obtained from SCWA sondes to calculate water density from the UNESCO (1981) Equation of State. Using this density, the height of water above the gage was calculated by assuming hydrostatic conditions. All four gages were referenced to the NGVD datum by comparing data with data from the SCWA gage at Jenner, which has been surveyed in to NGVD. By identifying a time during inlet closure (i.e., no tide) when river flow and wind are minimal, one can assume that the water surface is horizontal throughout the estuary and make direct comparisons between gages. Given the uncertainty involved in this method, the elevations estimated for the loggers are assumed to be accurate to within ±5cm, however, when considering changes in slope, this error cancels out and gages will have an accuracy as specified (i.e., <1cm).

2.2 – Boat-based CTD surveys

A Seabird SBE-19 profiler with an attached pump was used to obtain vertical profiles of temperature, salinity, density, dissolved oxygen, PAR and chlorophyll fluorescence versus depth. Data were logged at 4 Hz below about 10cm beneath the water surface. Locations of profile stations are shown in Figure 2.1. Further details on CTD data collection can be found in the data report (Behrens & Largier 2010).

2.3 – Time-series of vertical profiles of currents

Bottom-mounted ADCP's were deployed at Paddy's Rock and Heron Rookery (Figure 2.1). Each obtained a 10-minute average profile once an hour, resolving tidal and diurnal variability in currents. A vertical resolution of 0.25m was obtained at Heron Rookery and 1.0m at Paddy's Rock. Flow rates are calculated from combining velocity data with channel width estimates from the bathymetry data (see Section 2.5 below). Data were obtained at Paddy's Rock from 26 June to 24 July and at Heron Rookery from 26 August to 28 October.

2.4 – Time-series of water temperature and salinity

Seabird SBE-37-SM MicroCat recorders for temperature and salinity were deployed on the bottom of the estuary at three locations shown in Figure 2.1. One MicroCat was

attached to each ADCP, and a third one was located in a shallow channel adjacent to Freezeout Island, between the Heron Rookery and Freezeout Creek profiling stations. In addition, several YSI 6600 datasondes had been deployed by SCWA in May, recording data on temperature, salinity, pH, pressure and dissolved oxygen at near-surface, mid-depth and near-bottom depths (depending on location). At Paddy's Rock and Heron Rookery, the near-surface SCWA sondes were combined with near-bottom MicroCats to obtain top-bottom density differences used in stability calculations (Section 4.3). Mid-depth sondes at Sheephouse Creek, Heron Rookery and Freezeout Creek (as well as near-bottom sondes at Heron Rookery and Freezeout) were also used to monitor salinity intrusion during tidal conditions. The MicroCat deployed at Freezeout Island provided additional detail on intrusions of saline waters at depth.

Contour plots of the longitudinal distribution of temperature, salinity or dissolved oxygen is obtained by interpolating between profile locations using a cubic-spline interpolation scheme in MATLAB. The longitudinal depth profile is derived from the bathymetry. The entire set is presented in the data report, and examples are presented in Chapter 3. In this analysis, it is assumed that lateral structure is homogeneous (or nearly so), so that the 2-dimensional along-and-vertical contour plot is representative of the whole estuary. Lateral structure will be investigated in future work, specifically exploring differences between the channel center and shallow littoral waters.

2.5 – Estuary bathymetry

The high-resolution 2009 survey of estuary bathymetry (EDS, 2009) was used for this analysis. The continuous surface generated by PWA, using the triangular interpolated network (TIN) approach, was sampled to produce a 10m x 10m raster file. This grid was used to obtain a longitudinal thalweg profile for the estuary, and in calculation of stage-storage relations for the entire estuary and for individual reaches. These stage-storage relations are used in seepage calculations (Section 3.1) and in salt and dissolved oxygen budgets (Sections 3.7 and 3.8).

2.6 – Meteorological data

Meteorological data on wind speed, air temperature, barometric pressure and relative humidity were obtained from sensors at Bodega Marine Laboratory, approximately 12 miles south of the mouth of the Russian River. While wind speed may vary between BML and the mouth, the wind at the two locations is expected to be well correlated, with strong wind or calm conditions being experienced concurrently in this region (including the estuary closest to the mouth). More importantly, wind speed and direction varies along the estuary, with airflow generally following the valley orientation, but with some locations being sheltered by the adjacent hills. As such, BML wind data are used as an index of the importance of wind forcing. In contrast, it is expected that air temperature, barometric pressure and relative humidity vary little between BML and the Russian River mouth.

2.7 – Wave measurements

Deep-water wave height data were obtained from the CDIP Pt. Reyes Buoy (Buoy #29). These data were converted to estimates of wave height at the 10m isobath offshore of the Russian River mouth using a transformation matrix provided by CDIP. The matrix for converting offshore wave heights to nearshore values accounts for wave refraction and shoaling, and is described further in Battalio *et al* (2006) and Behrens *et al* (2009).

2.8 – River flow measurements

River flow data are available for the Russian River at Johnsons Beach at Guerneville (USGS Site 11467002) and also further upstream at Hacienda Bridge (USGS Site 11467000). As there are many opportunities for inflow or extraction between these sites and the head of the estuary, SCWA provided additional flow measurements at Vacation Beach, which is much nearer the upstream boundary of the estuary. Flow was measured using an impeller-based device at width intervals across the channel. Flow measurements were compared with water level measurements to provide a flow-stage relationship. Then a continuous water-level record was used and data interpreted as flow rates, based on the above relationship. These flow-rate estimates were used to determine the contribution of river flow to the estuary volume as part of the water budget model (Section 3.1).

3. Data Analysis

The results from several analyses are reported in this section. A full representation of the data is available in the companion data report (Behrens & Largier 2010). Here we address specific issues:
(1) An estimate is obtained for water lost as seepage through the sand barrier at the mouth by calculating a budget of water flow into and out of the estuary.
(2) Tidal flows and diurnal wind-driven seiche flows are quantified through an analysis of data on current velocities and water level fluctuations.
(3) The spatial distribution of salinity is described, specifically addressing intrusion of salinity upstream during open and closed periods.
(4) The spatial distribution of water temperature is described and changes during the long closure event are outlined.
(5) The spatial distribution of dissolved oxygen is described, identifying locations and times when anoxic or hypoxic conditions are found at depth.
(6) Stratification is quantified and analysis of the stability of this stratification provides a measure of the likelihood of mixing between deep saline water and surface freshwater.
(7) A salt budget is calculated for the long closure event.
(8) An oxygen budget is calculated for the lower layer.

3.1 – Water budget & Seepage analysis

At the heart of the NMFS-proposed management protocol for the Russian River estuary is the concept that water will escape from a closed estuary by seeping through the sand barrier that separates it from the ocean. This will happen due to the rise of the elevation of the estuary water level above that in the ocean (i.e., a scenario typically described as a “perched lagoon”). This “seepage loss” may be accompanied by a flow of water over the sand barrier (which is also known as the “berm”, referring to its wave-built origin). Such an “overflow” at the mouth of the Russian River is not common in recent times (PWA 2009), and the future flow rate is expected to be much lower than typical river inflow rates in the past, even in dry years, so that a significant seepage loss is required to maintain a steady water level in the estuary. Both overflow and expulsion of deeper saline waters through the sand barrier occur in comparable smaller estuaries along the coast of California, as noted in NMFS (2008).

3.1.1 – Historical closure events

In the past, closure events have often lasted several weeks without breaching, despite the lack of accommodation space for cumulative inflow. Without significant loss of water from the estuary, closures of the Russian River mouth would be short-lived: given river inflows on the order of 100 cfs, the estuary water level would reach stages in excess of 7ft NGVD29 within 1-2 weeks without some form of water loss. Extensive records of inflows near Guerneville and closure duration at the mouth indicate that several closures have endured much longer. This suggests that there is a significant export of water from the estuary that offsets inflow during closure events.

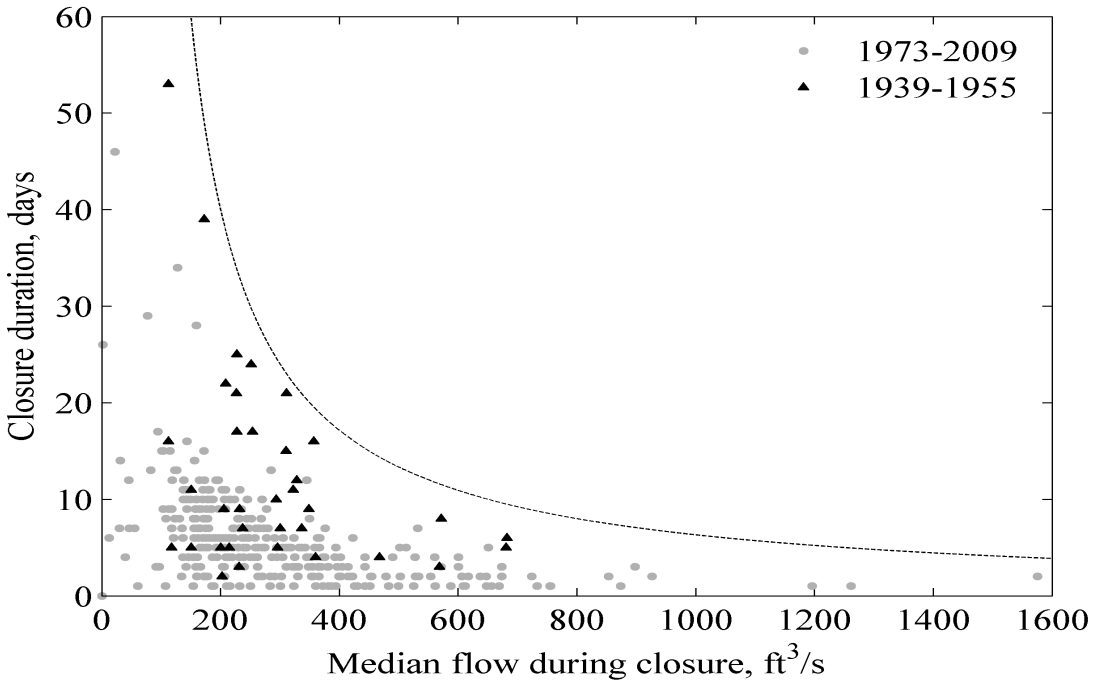

Figure 3.1. Closure durations and median flows observed by Rice (1974) and Behrens *et al.* (2009).

In Figure 3.1, closure duration is compared with median inflow for about 150 events spanning five decades. A DWR gage operated between 1939 and 1955 was used by Rice (1974) to infer closure events, while closure events after 1973 were observed directly by Elinor Twohy, a resident of Jenner (Behrens *et al.* 2009). The earlier record does not reflect all closure events, as the gage occasionally malfunctioned. One can see that closure durations tend to be much shorter during the more recent period, due to the D1610 decision in 1986 that required minimum summer flows combined with the

existing SCWA-management protocol that requires an artificial breach when Jenner stage exceeds 7ft NGVD29. Although local residents breached the barrier at times during the earlier period (Rice, 1974), they were less frequent – consistent with the observation of closures lasting much more than two weeks.

An interesting characteristic of these data is that for many of the closure events lasting for more than 20 days, the median flow was in excess of 70cfs (indeed many had inflows on the order of 100cfs or more). These closures could only persist if there were a concomitant loss of water from the estuary basin of the same order of magnitude. We use this principle in the next section to obtain an estimate of seepage rates.

3.1.2 – Estimation of seepage rate

An estimation of water loss from the estuary basin can be obtained by comparing inflows and outflows with changes in the volume of water in the basin, i.e., a water budget for the estuary. Equation (1) expresses this balance, explicitly listing all of the terms, which are illustrated in Figure 3.2. This budget treats the estuary as a box with well-defined lower and upper boundaries – the mouth and Vacation Beach, respectively. Measured bathymetry (EDS, 2009) was used to characterize the estuary shape and volume for different water levels (hypsometric curve). Budgets are constructed for all days when the mouth was closed during the ten-year period from 1999 to 2009.

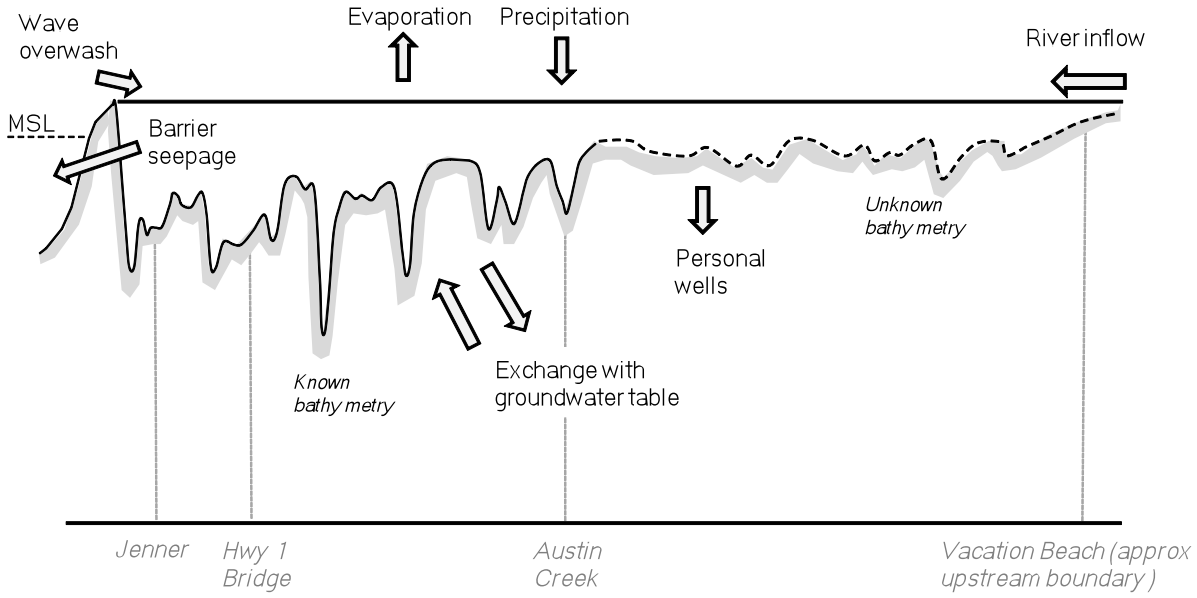

Figure 3.2. *Estuary schematic detailing processes relevant to changes in volume during closure ("personal wells" is synonymous with "domestic wells").*

Equation 1 shows that changes in the volume of water in the estuary must be explained by inputs (river inflow + wave overwash + precipitation on surface) minus outputs (evaporation across surface + seepage through the sand barrier + seepage into aquifers + extraction).

$$(dV/dt)_{estuary} = Q_{river} + Q_{overwash} + P - E - (Q_{seep} + Q_{aquifer}) - Q_{extract} \qquad \text{[Eq. 1]}$$

where V represents the estuary volume, t represents time, P and E are precipitation and evaporation rates, and Q represents a flow rate. Using a 24-hour time step, the rate of water added or subtracted from the estuary is estimated for each term, as described below.

1. *Change in estuary volume*: This was calculated from changes in water level, using the hypsometric curve calculated from EDS bathymetric data.

2. *River inflow*: This was quantified through a stage-flow relationship obtained by SCWA at Vacation Beach, to account for inputs and extraction from the river below the USGS Hacienda Bridge gage. This inflow assumes negligible surface inflow from Austin Creek and other smaller creeks that are below Vacation Beach. For higher flow rates that exceeded the range of data in this relationship, flows from the Hacienda Gage were used.

3. *Wave overwash*: This occurs rarely, as well-defined events. Days on which overwash is known to occur are excluded from this analysis, and it is assumed that overwash is negligible for other days.

4. *Precipitation*: Given that longer closures occur during the summer and fall seasons when rainfall is typically absent, precipitation is assumed to be zero. Rainfall records were used to confirm the absence of rain during the events analyzed here.

5. *Evaporation*: This was calculated using the method of Linacre (1992), which does not require continuous water temperature data. It is assumed to provide sufficient accuracy given that total evaporation losses were between 0 and 5cfs, one to two orders of magnitude less than river inflows (typically 70-300cfs) and calculated seepage losses (30-100cfs).

6. *Seepage loss*: This term refers to an outflow from the perched estuary through the sand barrier at the mouth. It is combined with the next term into a single unknown loss term.

7. *Loss to aquifers*: This term quantifies groundwater-surface water interactions and it can be positive (i.e., flux from estuary to aquifer) or negative (i.e., flux from aquifer to estuary). It is combined with the previous term into a single unknown loss term.

8. *Extraction*: Withdrawal of water is only via domestic wells within the model domain. This can be shown to be a negligible flow rate, considering typical rates of domestic water use.

Re-arranging Equation 1, one gets a simple expression for the combined unknown loss term $Q_{loss} = Q_{seep} + Q_{aquifer}$:

$$Q_{loss} = Q_{river} - E - (dV/dt)_{estuary} \qquad \text{[Eq. 2]}$$

There are no data on the flux of estuarine waters to local aquifers $Q_{aquifer}$ and thus this term is retained in the combined loss term, but it is expected that Q_{loss} is primarily due to the seepage term and these terms are used interchangeably in the following discussion.

Unknown bathymetry

High-resolution bathymetry data are available as far upstream as the confluence with Austin Creek, and some distance into Jenner Gulch, Willow Creek and Freezeout Creek, but bathymetry is poorly known upstream of Austin Creek. In closure periods, water levels can rise as far upstream as Vacation Beach, about 10 km above Austin Creek.

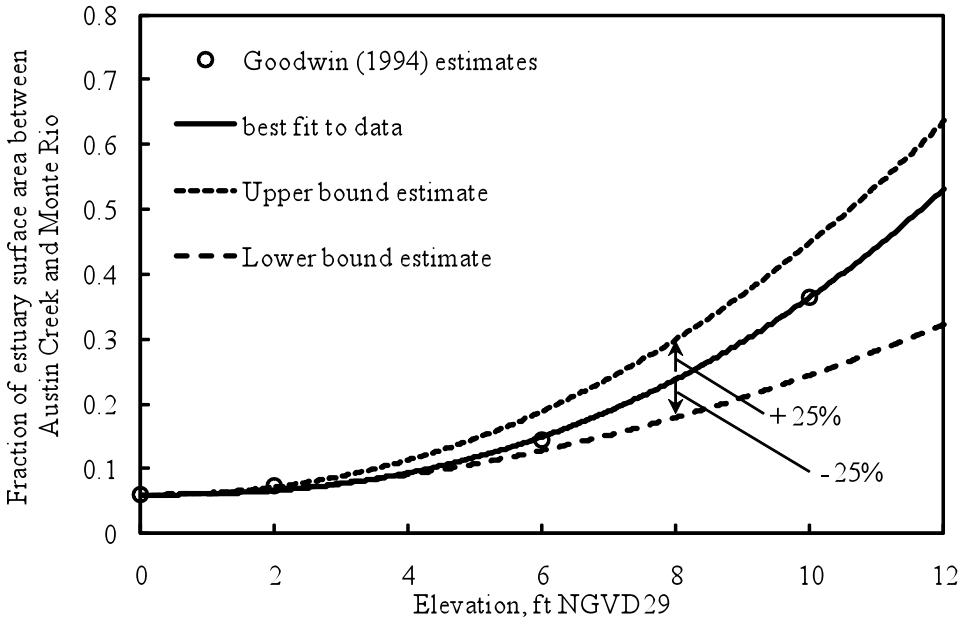

Figure 3.3. *Comparison of estimates for estuary surface upstream of Austin Creek*

Bathymetry in this reach was estimated from channel profiles measured by Goodwin & Cuffe (1994). The relative importance of backing up water upstream of Austin Creek was assessed by corrections to the hypsometric curve, expressing surface area in this "upper" reach as a fraction of total area (Figure 3.3). The best fit to Goodwin and Cuffe's data is shown as well as 25% errors as upper- and lower-bound estimates, which are expected to bound the unknown real values.

As shown in Figure 3.4, a 25% uncertainty in the volume upstream of Austin Creek introduces a small error in quantifying the total estuary volume (error is order 1% at 8ft NGVD). This is because significant amounts of water do not backup into this region until the estuary stage is high. Even at 8 ft NGVD this uncertainty accounts for no more than a 2cfs error in estimates of loss.

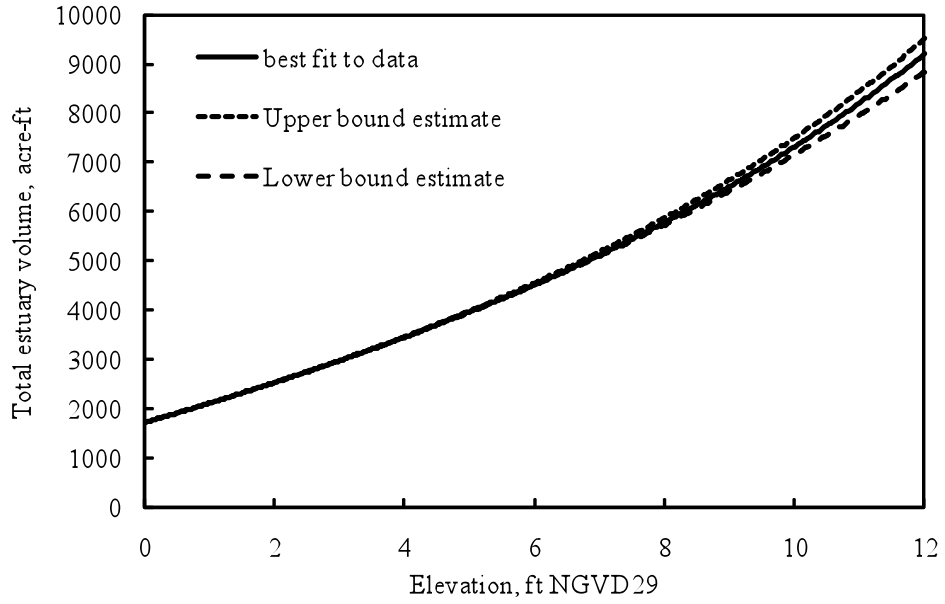

Figure 3.4. *Estuary stage-volume relation comparing methods of estimating upstream surface area*

Wave overwash

Data recorded during the September 2009 closure event and other historical events have shown a sudden increase in estuary water level during periods of high waves. For example, between September 12 and 14 the water level in the estuary rose 0.4m (~1.5ft) during a prolonged period with nearshore wave heights exceeding 4m (see

Figure 3.7). A concurrent drop in estuary temperature and increase in the mass of salt in the estuary salt mass (see Figure 3.39) indicate that wave overwash was indeed the cause of the water-level change. As wave-overwash volumes are difficult to estimate without direct data, or data on berm morphology (e.g. height, width), these days were excluded from water budget calculations. Days were excluded if wave heights exceeded 1.2m (~4ft) or if wave heights exceeded the difference between estuary and ocean levels by more than 0.3m (~1ft).

3.1.3 – Relation between seepage loss and water level

The loss of water owing to seepage through the sand barrier at the mouth is driven by the pressure difference across the barrier due to the difference in water level between estuary and ocean. The rate of flow Q_{seep} is expressed by Darcy's Law:

$$Q_{seep} = K.A.dh/dL \qquad \text{[Eq. 3]}$$

where K is the hydraulic conductivity (related to permeability of the barrier), A is the cross-sectional area of the flow through the barrier, and dh/dL is the hydraulic gradient (hydraulic head divided by length of flow path). Thus, as the estuary water level rises one expects the seepage rate to increase (given that ocean water level changes little at time scales longer than tidal).

Here the loss term from Equation 2 is plotted against the difference between Jenner-gage estuary water level and 25-hour averages of the sea level at the Pt. Reyes tide gage (Figure 3.5). The difference Δh produces a better fit with flow loss estimates than the Jenner gage level alone, because the sea level is not constant but varies in response to winds and waves (Largier *et al* 1993; O'Callahan *et al* 2007), which have a different local effect on the beach at the mouth of Russian River than they do on the headland at Point Reyes.

Since Point Reyes measurements do not reflect local winds, nor short-period wave generation in the vicinity of the Russian River mouth, nearshore significant wave heights may be underestimated at times. This makes it difficult to exclude all events when wave overwash may have occurred – resulting in some points that may be in error (discharge lower than expected for given hydraulic head). However, as the beach height increases, wave overwash becomes less common (e.g. Donnely *et al* 2006) and this potential error is unlikely to be an issue. For these reasons, some outlier data obtained from days of intense wind or waves were excluded from Figure 3.5.

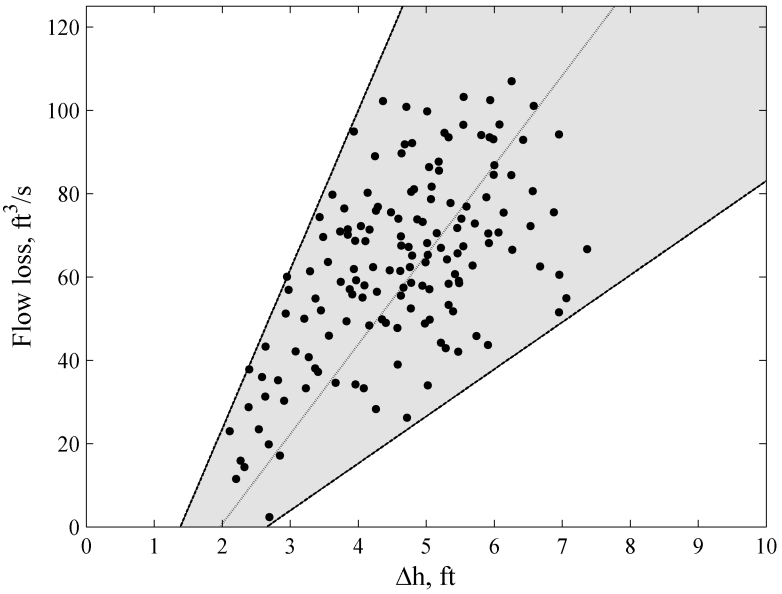

Figure 3.5. *Flow loss related to the difference between estuary and ocean water levels for all closure events between 1999 and 2009.*

Despite the scatter in the data, there is a clear trend, indicating an increase in losses from the estuary as Δh increases. The best linear fit to the data is given by:

$$Q_{loss} = 21.5\Delta h - 42.4 \qquad \text{[Eq. 4]}$$

where flow loss is in units of cfs, and Δh is in units of feet. The rms error for this relationship is ± 22.9 cfs. The scatter in data is due to errors in the method of estimating Q_{loss} as described above, and also due to seasonal and interannual differences in surface-groundwater fluxes which are not expected to relate simply to estuary-ocean hydraulic head. For a given event, there is typically less scatter as surface-groundwater fluxes are expected to change more slowly than the estuary-ocean hydraulic head.

Perhaps more important for operational purposes is the lower bound, which provides an empirical estimate of the minimum flow observed for a given estuary stage:

$$Q_{loss} = 11.3\Delta h - 30.0 \qquad \text{[Eq. 5]}$$

And the maximum flow observed for a given stage is given by the upper bound:

$$Q_{loss} = 38.2\Delta h - 53.0 \qquad \text{[Eq. 6]}$$

Histograms of the probability of flow rates for a given hydraulic head (Figure 3.6) provide more insight to this relation. Although there is a monotonic increase in mean seepage rate with increased elevation head, the increase is greatest as elevation head increases from 2-3ft to 3-4ft. For the remaining Δh brackets, the increase in seepage is notably smaller. Although this may be an error because wave-overwash events were not successfully excluded for lower elevation heads, this is not a problem for the estimates at higher elevations.

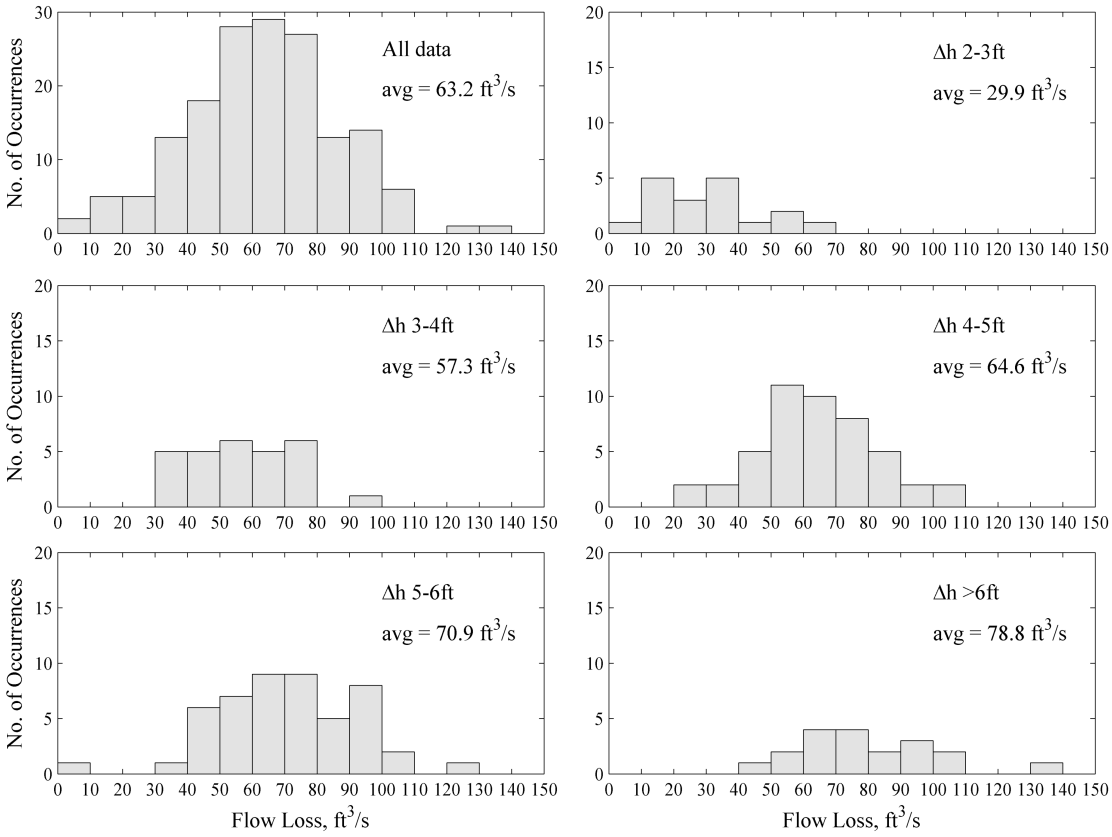

Figure 3.6. *Distributions of estimated flow loss at various differences between estuary and ocean water levels (Δh).*

The exact nature of the stage-discharge curve for seepage is likely to be non-linear and may be quite complex. For example, the sudden increase in flux as stage rises past 3ft suggests that a horizon of high conductivity is found at this level (e.g., permeable rip-rap used as a foundation for the jetty). However, any decrease in conductivity at higher elevations is countered by an increase in hydraulic gradient due to narrowing of the

berm towards its crest (decreasing ΔL) – so that discharge should increase more rapidly with stage than would be expected from a linear relation due only to increasing Δh.

There are further complicating factors. For example, in general one expects an increase in seepage rate during a flow event, due to increased hydraulic gradient and increased cross-sectional area. However, when wave overwash persists one may see a decrease in seepage rates due to an increase in beach width resulting from wave-overwash sediment transport over the berm during closure events (Donnely *et al* 2006).

Seepage flow losses from an estuary are influenced by (1) the properties and thus permeability of berm sediments, (2) beach morphology, and (3) groundwater elevations. The latter two in particular can vary sharply among seasons. Beaches tend to be widest in summer and narrowest during the winter (Komar 1997). This would lead to lower seepage rates during the summer and higher seepage rates in the winter. However, water tables are highest in late winter months and increased inflow or reduced losses at this time would counteract enhanced flow loss through the berm. Analysis of individual closure events (Figures 3.7 and 3.8) shows large differences in the seepage rate among closures, even during the same season.

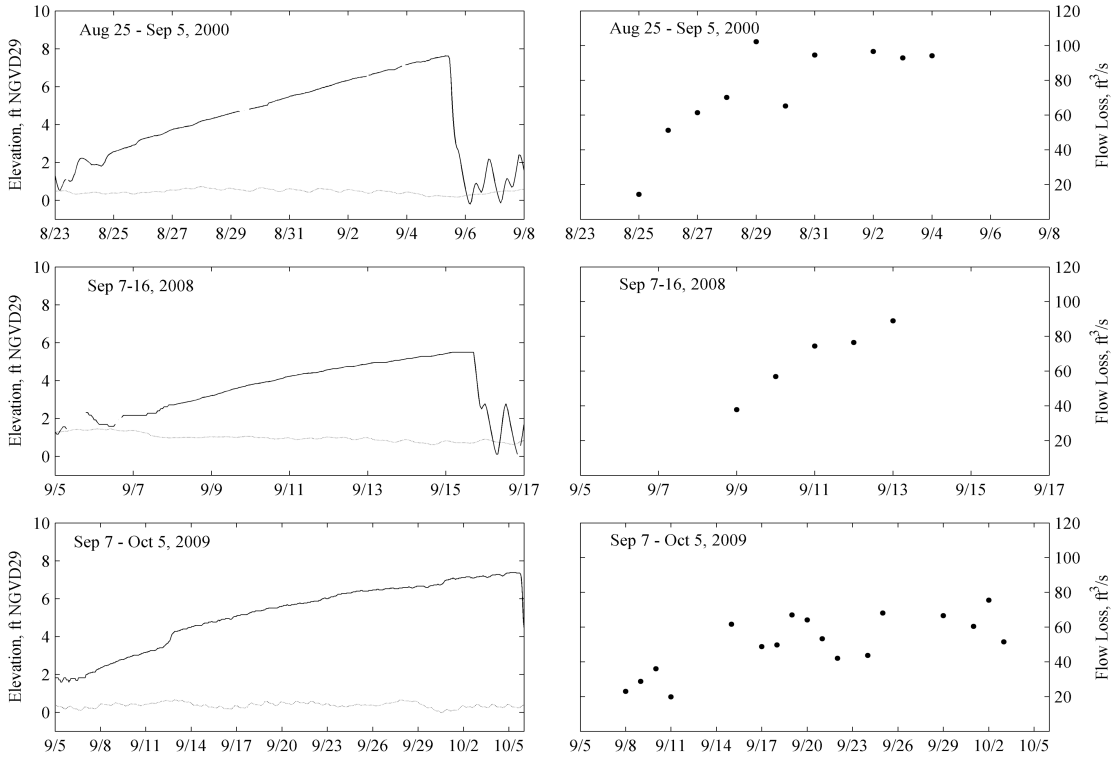

Figure 3.7. *Observed flow losses during fall closure events. Dashed line represents 25-hour moving average of Pt. Reyes levels.*

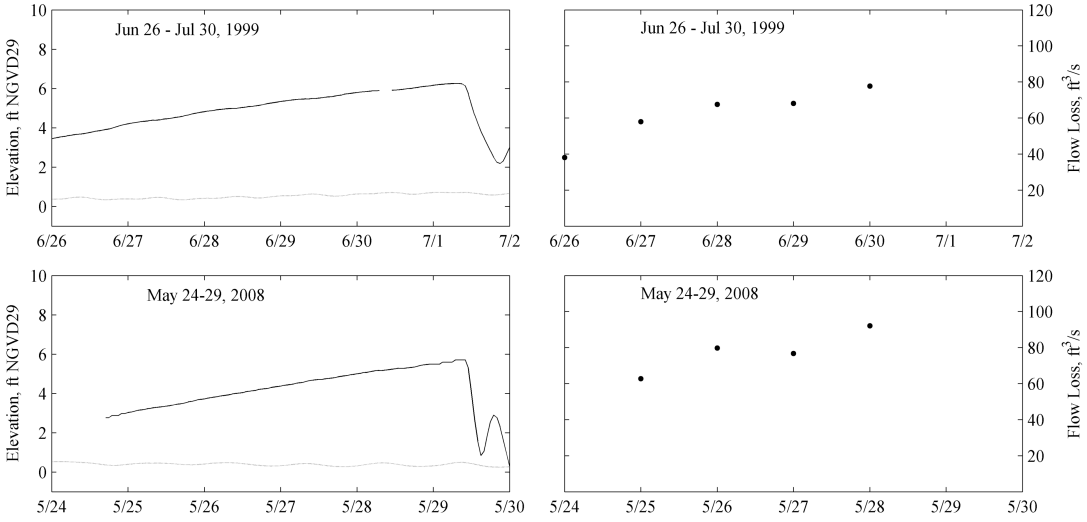

Figure 3.8. *Observed flow losses during spring closure events. Dashed line represents 25-hour moving average of Pt. Reyes levels.*

It is interesting to note that water level in the estuary may asymptote to a steady level as increased losses due to seepage match steady river inflow, e.g., at the end of the September 2008 event and at the end of the September-October 2009 event. This is not observed in the other events, when inflows are larger. Another phenomenon appearing in the 2009 event and also in the August-September 2000 event is a leveling off of the flow loss term over time (or with elevated water level).

While understanding the observed stage-discharge relation (Figure 3.5) and specific events (Figures 3.7 and 3.8) needs further attention, the lower bound on a decade of empirical results (Figure 3.5; Equation 5) provides a sound basis for operational estimates of minimum water loss rates for given water level elevations.

3.2 – Tidal and diurnal currents

Observed currents are dominated by strong tidal flows throughout the water column when the mouth is open and by weak wind-driven flows near-surface when the mouth is closed. Owing to instrument malfunction, data are only available from Paddy's Rock during open periods dominated by tidal flows whereas for much of the time that the

ADCP was deployed at Heron Rookery the mouth was closed. A full record of currents at both sites is plotted in the data report of Behrens & Largier (2010), showing variations in the strength of tidal currents over the spring-neap cycle and also over the cycle of mouth closure. In the following subsections individual profiles are plotted to best illustrate a variety of flow phenomena that are of interest.

3.2.1 – Current velocities at Paddy's Rock

Paddy's Rock is 2.5km from the mouth, well within a tidal excursion of the mouth so that tidal intrusions of seawater are seen here daily. Circulation is dominated by the tides, with the strength of currents varying in response to the strength of the tide. Representative data are plotted below for days on which the tidal range was ~1ft, ~3ft, and ~5ft respectively (Figures 3.9, 3.10, 3.11). Current speeds over 30cm/s are observed during spring tides, whereas speeds may remain below 10cm/s during neap tides.

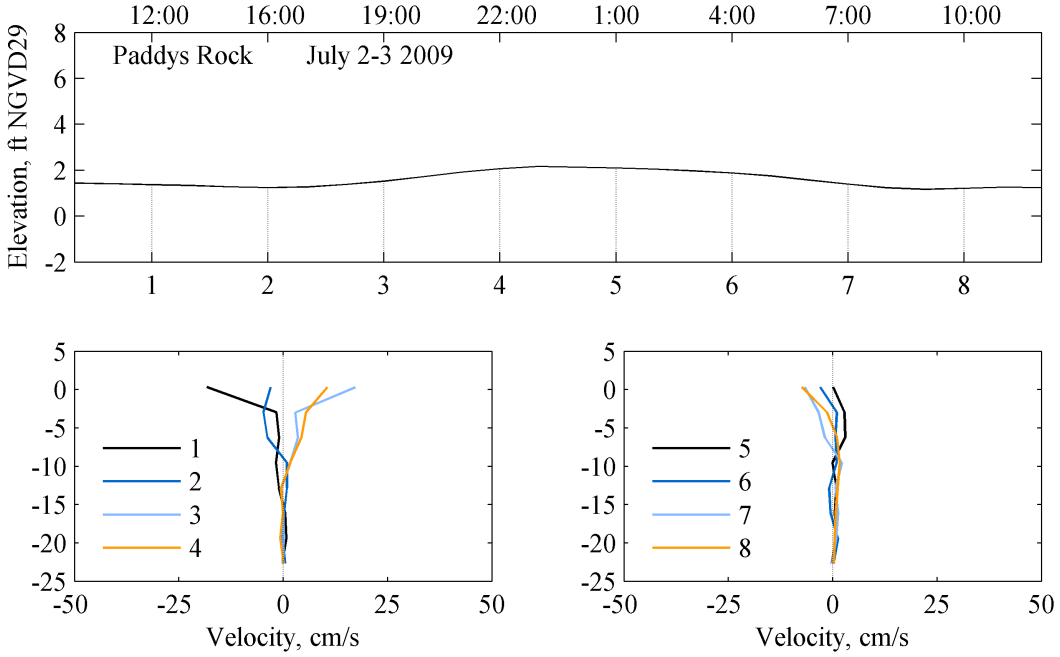

Figure 3.9. *Water levels (top panel) and profiles of along-channel speed versus depth (bottom panels) at Paddy's Rock on 2-3 July 2009, during a tidal cycle with ~1 ft range and 110 cfs river flow at Guerneville. Negative velocities indicate flow toward the mouth.*

Currents on 2-3 July 2009 (Figure 3.9) were very weak, except near-surface during the afternoon of 2 July. An outflow of about 20cm/s was observed in the uppermost 1ft, probably representing the seaward flow of a thin layer of river water which can slide

easily over denser estuarine waters in the absence of tidal and wind mixing. Later in the afternoon, during the weak flood tide, an inflow of 5-20cm/s was observed extending several feet down from the surface. While supported by the tide, this surface-amplified inflow is primarily due to an afternoon/evening sea-breeze that is felt on the estuary between Paddy's Rock and the mouth.

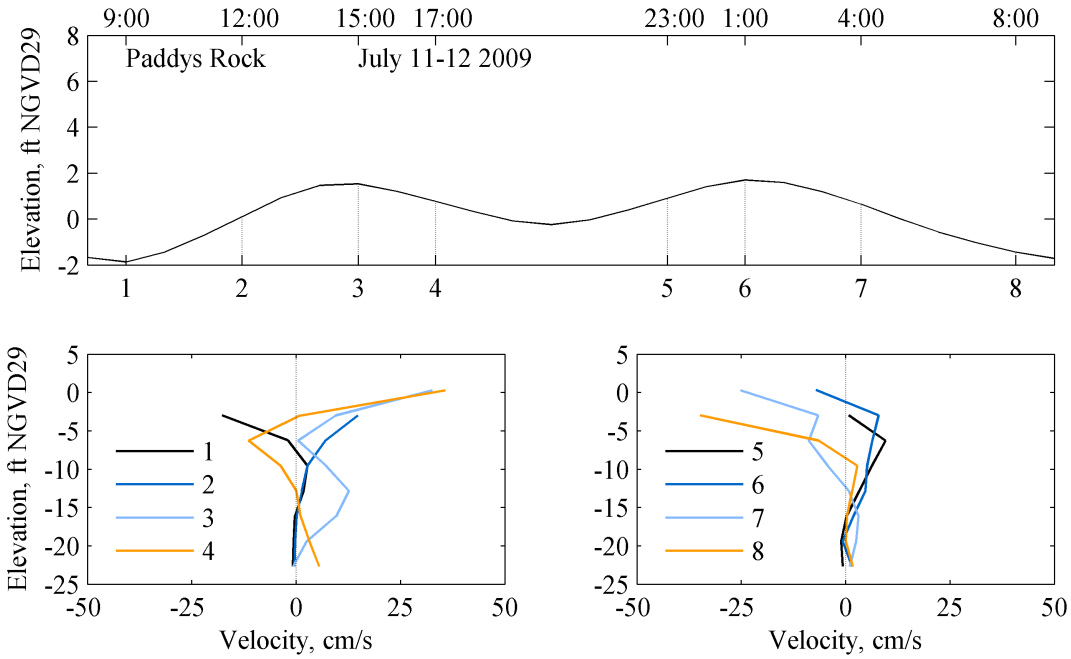

Figure 3.10. *Water levels (top panel) and profiles of along-channel speed (bottom panels) at Paddy's Rock on 11-12 July 2009, during a tidal cycle with a range of ~3 ft and Guerneville river flow of 110 cfs. Negative velocities indicate flow toward the mouth.*

Along-channel currents on 11-12 July 2009 (Figure 3.10) are stronger and observed throughout the 22ft-deep water column, with an intriguing vertical structure. At low tide on the morning of 11 July, a 5ft layer of low-salinity water is observed to be flowing seaward. This reverses to an inflow over the uppermost 10ft during the subsequent flood tide. However, by the time of the afternoon ebb tide, the afternoon sea-breeze has started and the 17h00 profile shows the uppermost 2ft moving landward due to surface wind stress while the waters between 2ft and about 12ft depth are seen to move seaward due to barotropic tidal pressure gradients. Below this, the near-bottom waters are moving landward (establishing a 3-layer flow structure, with mid-depth waters flowing seaward between surface and bottom waters). This sub-pycnocline inflow is also evident in the 15h00 profile and most dramatically seen in the profile at spring high tide

(Figure 3.11). This is due to baroclinic tidal pressure gradients, i.e., owing to differences in water density. During flood tide the outer estuary is filled with dense seawater (cold and salty) that then intrudes as a lower-layer flow during high tide and into the subsequent ebb tide. The nighttime flood tide is weak whereas the strong ebb tide in the dawn hours of 12 July (with no opposing wind) results in seaward flows of over 25cm/s extending to depth.

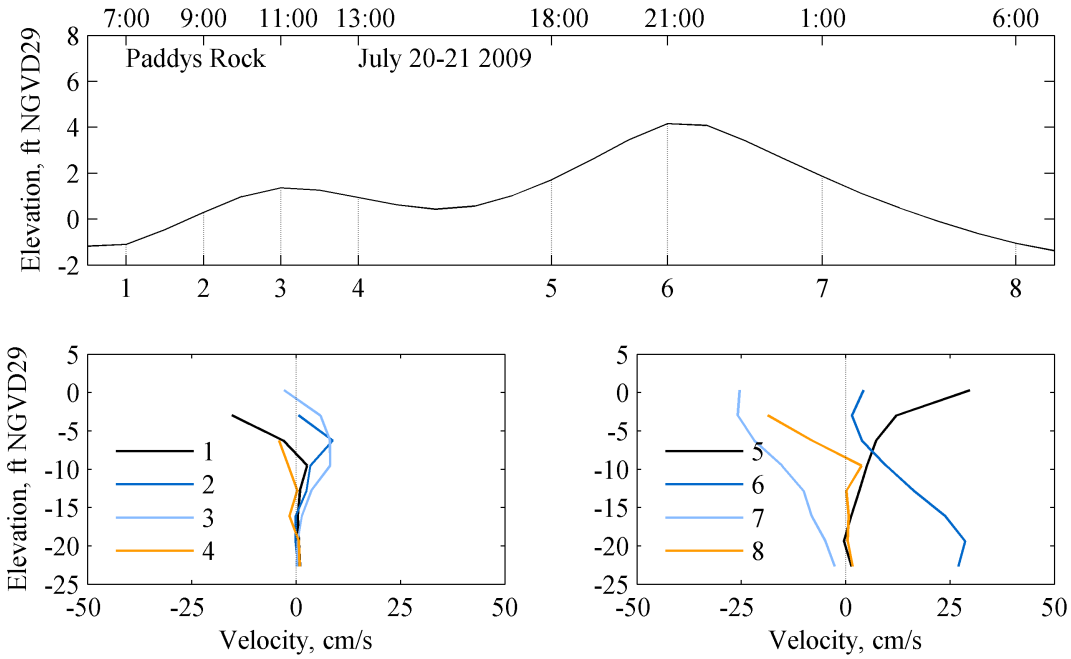

Figure 3.11. *Water levels (top panel) and profiles of along-channel speed (bottom panels) at Paddy's Rock on 20-21 July 2009, during a tidal cycle with a range of ~5 ft and Guerneville river flow of 62 cfs. Negative velocities indicate flow toward the mouth.*

The strongest currents are observed during spring tides on 20-21 July 2009 (Figure 3.11) and these currents exhibit thicker layers, often extending throughout the water column due to the enhanced vertical mixing during spring tides. The strong tidal currents start with an inflow in the evening of 20 July, with enhanced flow at the surface at 18h00 due to surface wind stress (but counter to baroclinic forcing). The high-tide profile at 21h00 shows a strong inflow of the dense lower layer due to baroclinic forcing as described above. This feature can be seen repeated every tidal cycle, and it is strongest during spring tides (Behrens & Largier 2010). While the flow has turned to seaward by mid-ebb (01h00 on 21 July), the baroclinic forcing counters this and explains weak flows below the pycnocline.

3.2.2 – Current velocities at Heron Rookery

Heron Rookery is 7.4km from the mouth, well beyond a tidal excursion of the mouth and typically beyond the reach of salinity intrusions during stronger river flow. However, during the low-flow summer and fall seasons in 2009, saline waters were observed at depth at Heron Rookery – sometimes trapped there and no longer connected to the main body of saline waters in the outer estuary. Tides and winds are also important here. Representative data are plotted below for days on which the tidal range was ~3ft, ~1ft, 0ft and ~4ft respectively (Figures 3.12, 3.13, 3.14, 3.15) – with range varying as a result of ocean tides and mouth constrictions. Current speeds over 30cm/s are observed during spring tides and near-surface during all conditions.

Currents in the evening of 28 August 2009 (Figure 3.12) are moderate, with an inflow of 10cm/s extending down to about 12ft during the late flood tide. On the subsequent 3ft ebb tide, seaward flows are over 20cm/s above the pycnocline at about 7ft; a strong shear is observed with currents zero a foot lower, immediately below the pycnocline.

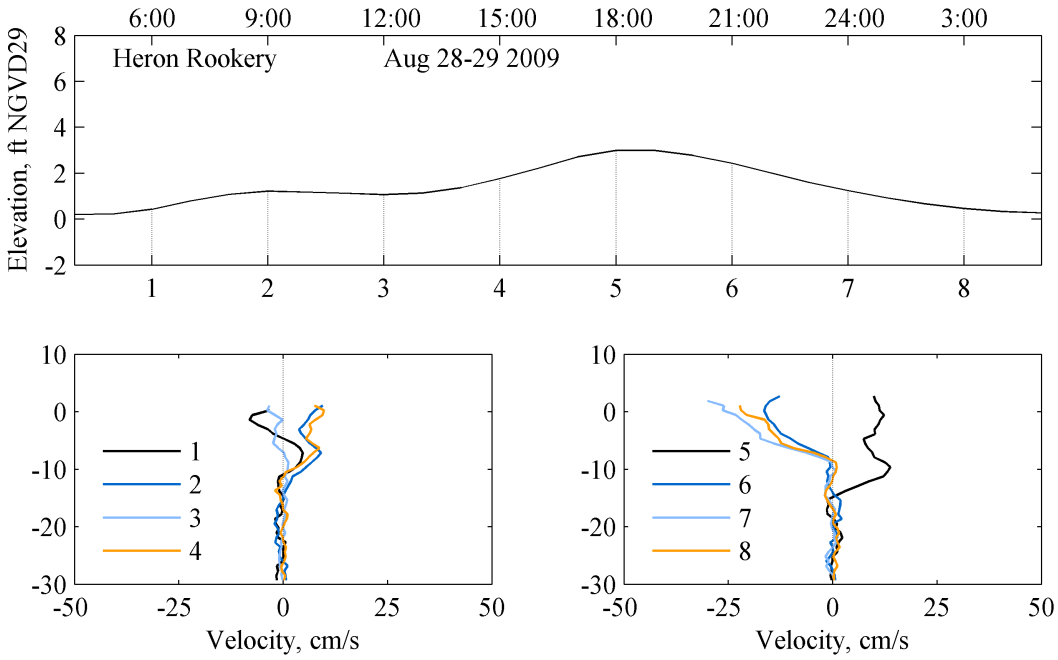

Figure 3.12. *Water levels (top panel) and profiles of along-channel speed (bottom panels) at Heron Rookery on 28-29 August 2009, during a tidal cycle with a range of ~3ft and Guerneville river flow of 63 cfs. Negative velocities indicate flow toward the mouth.*

Data for 3-4 September are obtained shortly before the mouth closes and the tide is constricted to a 1ft range at Heron Rookery. Near-surface landward flow is observed during the afternoon of 3 September, due to sea-breeze effects. By 19h00 a seaward flow is developing below the dissipating effect of surface wind stress. The weak ebb tide in the morning of 4 September, combined with river flow and baroclinic forcing results in a marked seaward flow at 07h00 with speeds of 10-20cm/s extending down to the pycnocline at about 5ft. In all profiles, there is negligible flow beneath the 5ft pycnocline.

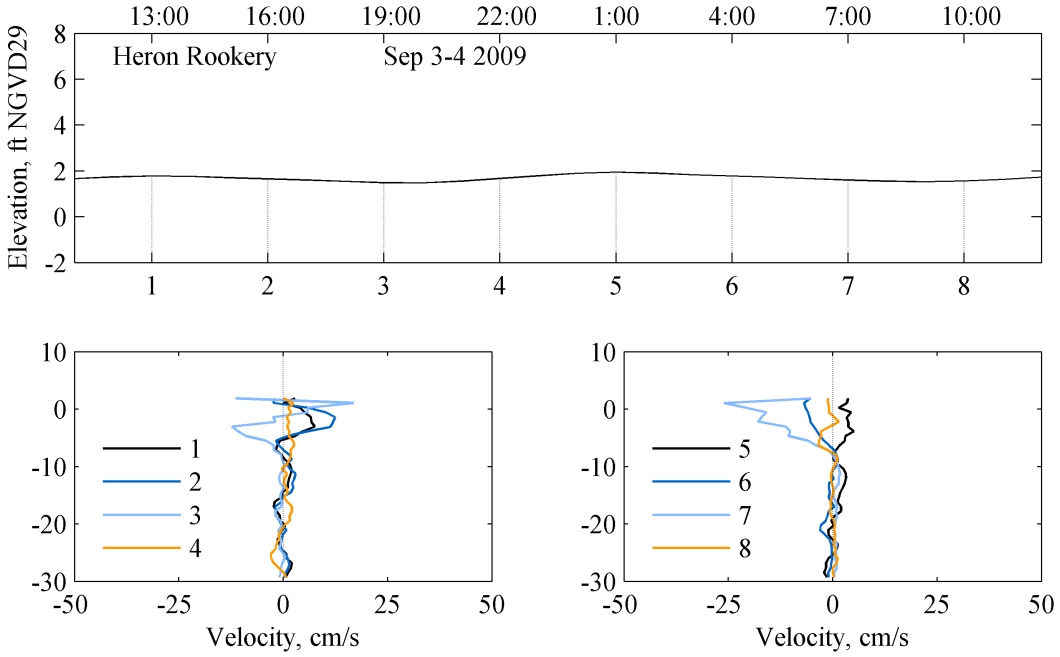

Figure 3.13. *Water levels (top panel) and profiles of along-channel speed (bottom panels) at Heron Rookery on 3-4 September 2009, during a tidal cycle with a range of <1ft and Guerneville river flow of 70 cfs. Negative velocities indicate flow toward the mouth.*

The mouth is closed on 23-24 September (Figure 3.14) and river flow is weak, so that currents are primarily wind-driven. A wind-driven landward flow is strongest at 13h00, but evident already at 10h00. By 16h00 the seaward pressure gradient due to river inflow and a day of landward wind forcing has started to overcome the effect of wind at depth and a layer between 5 and 10ft below the surface is seen flowing seaward while persistent wind forcing maintains landward flow of surface waters. By 22h00 the wind has gone and a weak seaward flow is observed over the uppermost 8ft. Again, flows below the 10ft pycnocline are negligible.

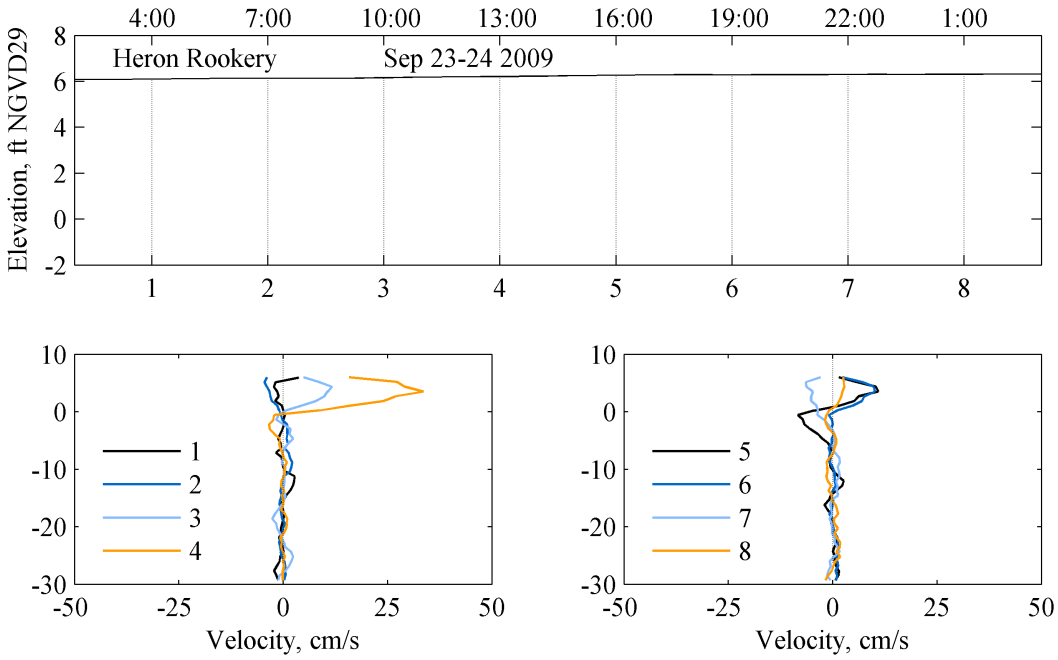

Figure 3.14. *Water levels (top panel) and profiles of along-channel speed (bottom panels) at Heron Rookery on 23-24 September 2009, during period of closure (tidal range 0ft) and Guerneville river flow of 74 cfs. Negative velocities indicate flow toward the mouth.*

The mouth is again open and river flow has increased by the time data was collected on 17-18 October (Figure 3.15), although a layer of salt water appears to remain trapped at depth (Behrens & Largier 2010). With strong tides and river flow, the water column mixes and currents are seen throughout the water column (except below the pycnocline 5ft from the bottom), reversing with the phase of the tide. Strong outflow is seen at 03h00 and strong inflow at noon and midnight. Strong outflows are again seen on the ebb tide in the afternoon, but both the 15h00 and 18h00 profiles exhibit the effects of landward wind forcing (and the absence of flow in the near-bottom saline layer).

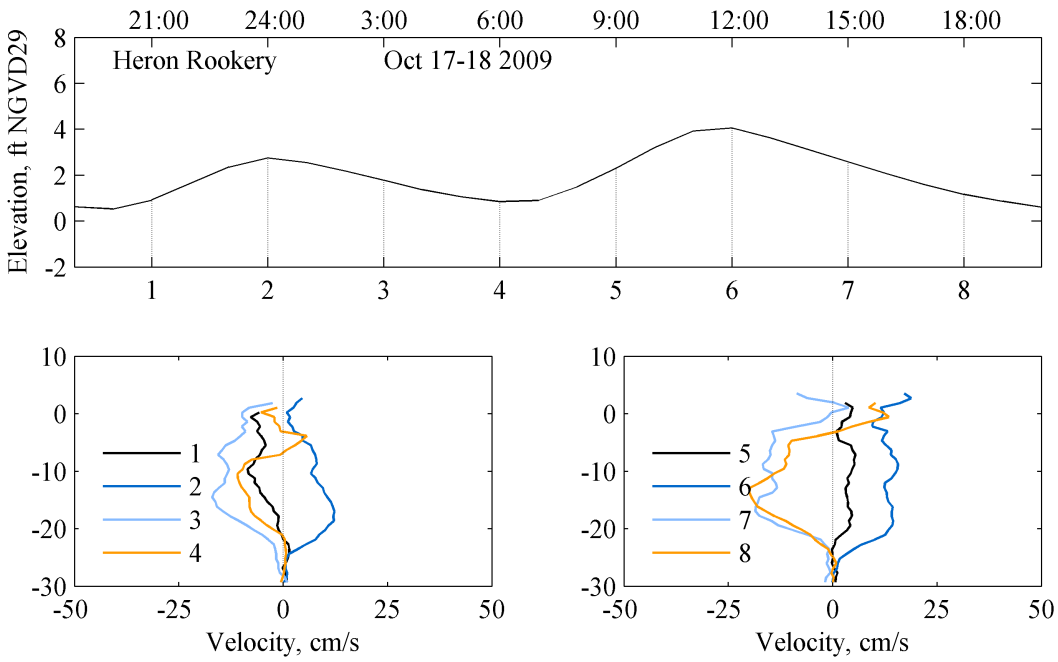

Figure 3.15. *Water levels (top panel) and profiles of along-channel speed (bottom panels) at Heron Rookery on 17-18 October 2009, during a tidal cycle with a range of ~4ft and Guerneville river flow of 296 cfs. Negative velocities indicate flow toward the mouth.*

3.2.3 – Diurnal wind-driven seiche

During mouth closure, surface wind stress drives the most noticeable along-channel currents in the Russian River estuary. As is common along the California coast, afternoon sea breezes blow from the cold ocean towards the warm interior. Where valleys funnel these winds, wind speeds are often over 10kts and may even exceed 20kts at places and times. Although quantitative data are not available, field notes confirm that this phenomenon occurred reliably in the Russian River estuary valley during the 2009 field study. The sea breeze may start as early as 10h00, typically peaks in the late afternoon (around 16h00), and then dissipates after sunset, lasting until 21h00 in June and July. While some reaches of the estuary are sheltered, the outer estuary is exposed to the strongest winds and the inner estuary is also subject to significant diurnal winds (specifically from Heron Rookery to Moscow Road bridge). A slope in the water level is setup by wind stress, so that even where the surface is sheltered the water level may be elevated.

This diurnal cycle in winds results in a setup of water level towards the back of the estuary during the afternoon as a result of the movement of near-surface waters that are directly forced by surface stress. Under some circumstances a pressure-driven return flow may develop at depth, beneath the direct effect of the surface stress. Nevertheless, the water level setup will remain as long as the wind blows. However, as the wind weakens, a landward flow will develop as the setup relaxes. This wind-driven seiche is clearly seen in water level data (Figure 3.16): around noon one can see the mouth water level dropping while the water level at Freezeout Island increases. A weaker increase in water level is also seen at Heron Rookery and a barely perceptible increase at Willow Creek (which must be near the pivot point for the water surface). As the sea breeze dissipates the slope in the water level relaxes, and may even tilt the other way during the night (e.g., early hours of 4 October). This forced seiche recurred daily. This wind forcing is also active during tidal periods, but the signal is swamped by tidal motions.

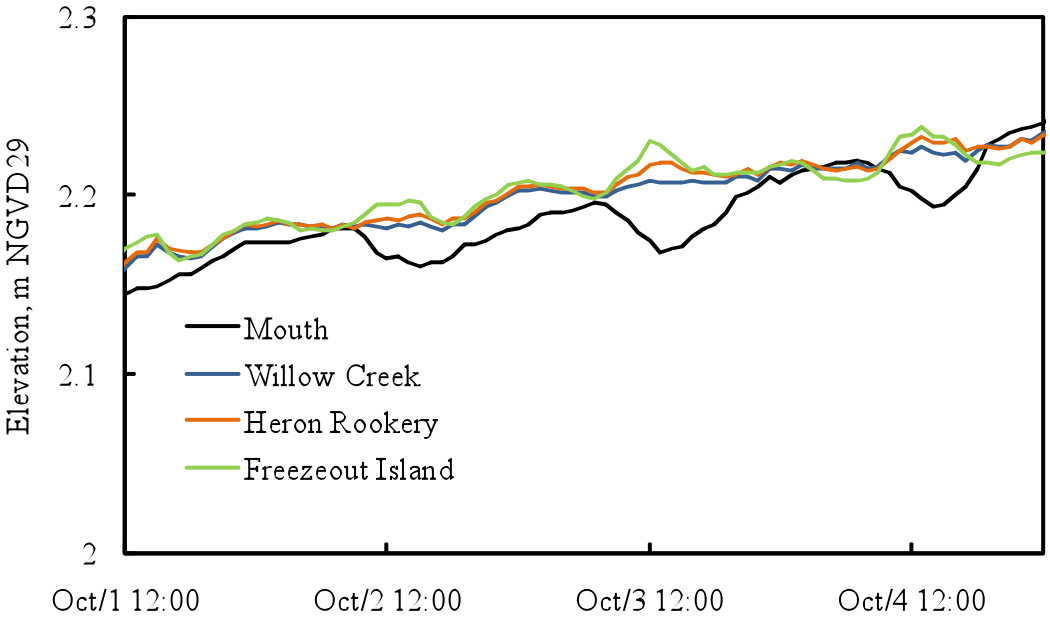

Figure 3.16. *Diurnal fluctuations in water level at 4 stations during inlet closure.*

The strength of transport associated with this seiche may be calculated either from water level data or from ADCP current velocity data. Water level measurements and estuary bathymetry were used to estimate the volume of water displaced upstream – the volume of water lost from the outer estuary should be equivalent to the volume gained by the inner estuary. At the same time, an estimate of the volume displaced past Heron Rookery is obtained by multiplying velocities measured at each depth by the channel

width at that depth and the vertical bin size (0.25m). Channel widths are obtained from the EDS (2009) bathymetry. A correction factor was applied to account for the difference between ADCP-measured flows mid-channel and the width-averaged flows at each depth. A correction factor of 0.6 was used, based on the assumption of a parabolic flow profile typical of a fully turbulent channel flow. The results are shown in Figure 3.17.

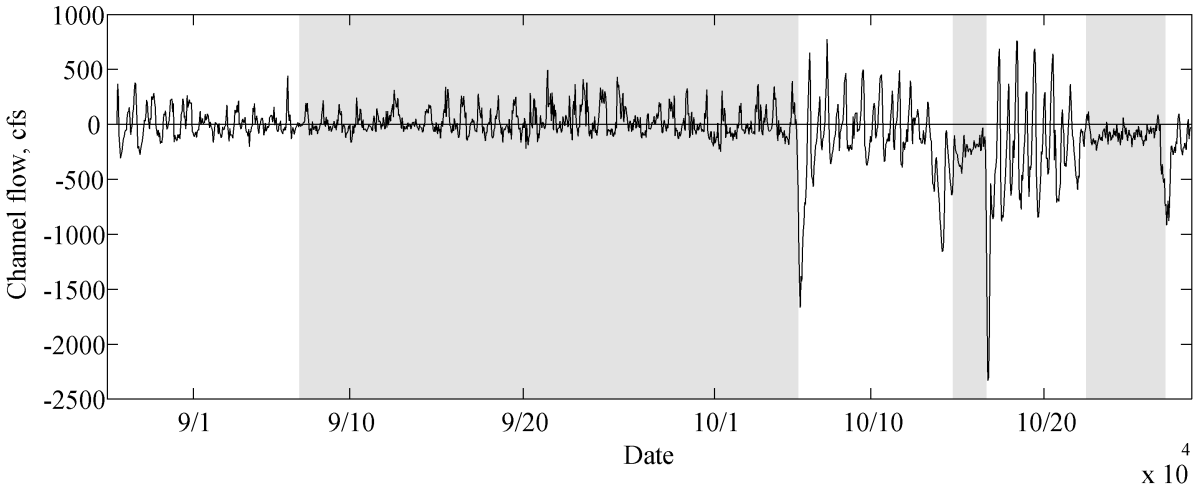

Figure 3.17. *Net transport at Heron Rookery calculated from integrating ADCP data cross-channel as described in the text. Positive flows are directed upstream. Shading indicates closure periods.*

Results from the two methods are compared in Figure 3.18. The estimates vary significantly in magnitude, but there is a reasonable qualitative agreement (in spite of the fact that these two methods assess transport in different locations). The errors involved in calculating flow from changes in volume are expected to be larger than those resulting from extrapolating ADCP measurements. This can be attributed to non-uniform wind speeds throughout the estuary, as well as errors involved in characterizing water levels and estuary bathymetry. The ADCP-derived transport shows that the wind-driven flow is short-lived, lasting less than a quarter day, with a longer slower relaxation flow. The water-level-derived transport shows an earlier start to upstream transport, which is expected given that this whole-estuary approach will be assessing flow at the pivot point, which appears to be just seaward of Willow Creek (see Figure 3.16), and the wind-driven setup can be expected here first.

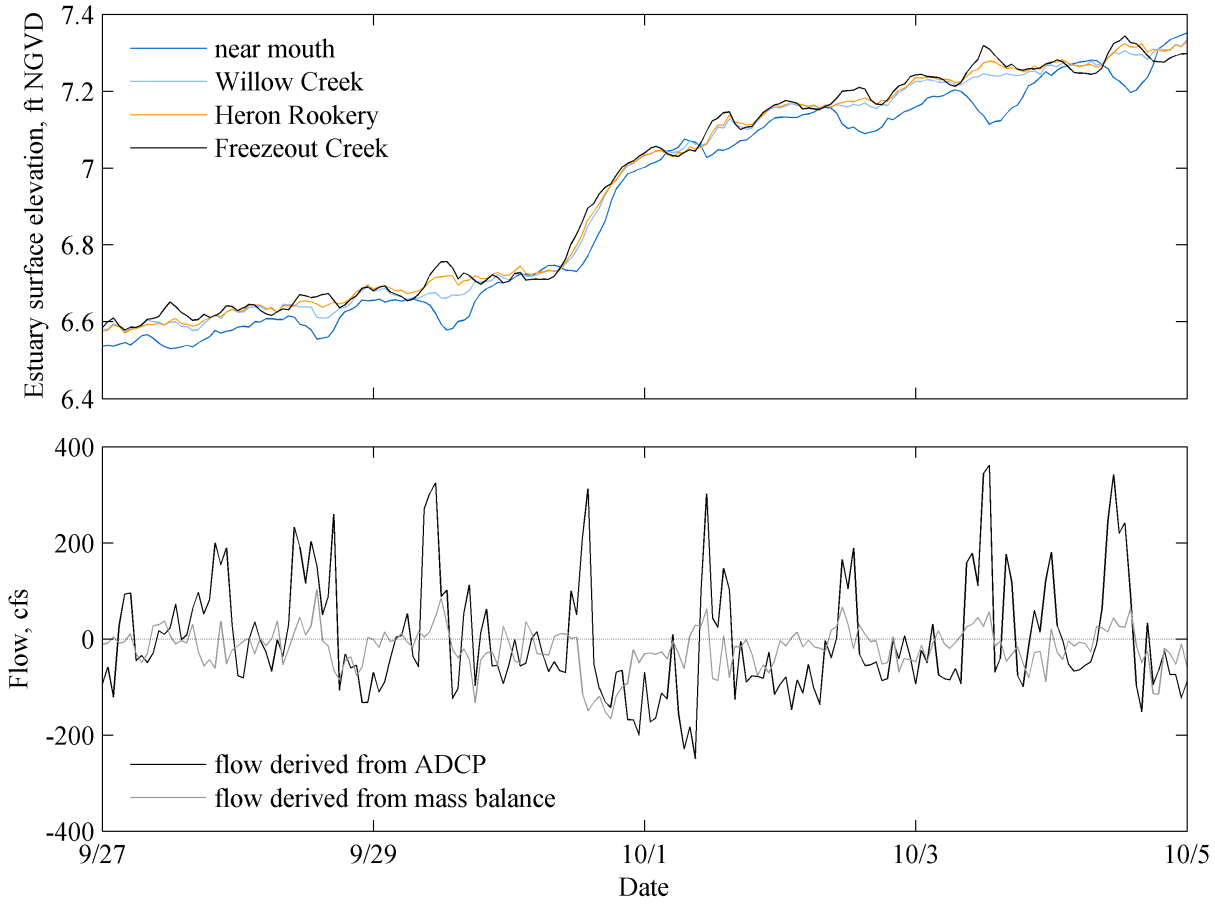

Figure 3.18. *Observed water levels (top panel) and corresponding flow rates calculated from water levels (lower panel, fine line) and from ADCP at Heron Rookery (lower panel, bold line) during the 2009 closure. Positive flows are oriented upstream.*

The flows associated with this seiche are evident in a contour plot of velocities at Heron Rookery during the September 2009 closure (Figure 3.19). Bursts of up-estuary flow in the uppermost meter are evident as orange-red, while prolonged relaxation overnight is evident as light blue. On closer inspection, one can see reverse flows below this wind-influenced surface layer. Between 1m and 2m one can see a seaward flow develop during the afternoon and also one can often see a landward flow beneath the seaward relaxation. These suggest that the phenomenon is not entirely forced and that some aspects of a true seiche are apparent. Beneath the pycnocline at 2m, currents are near-zero.

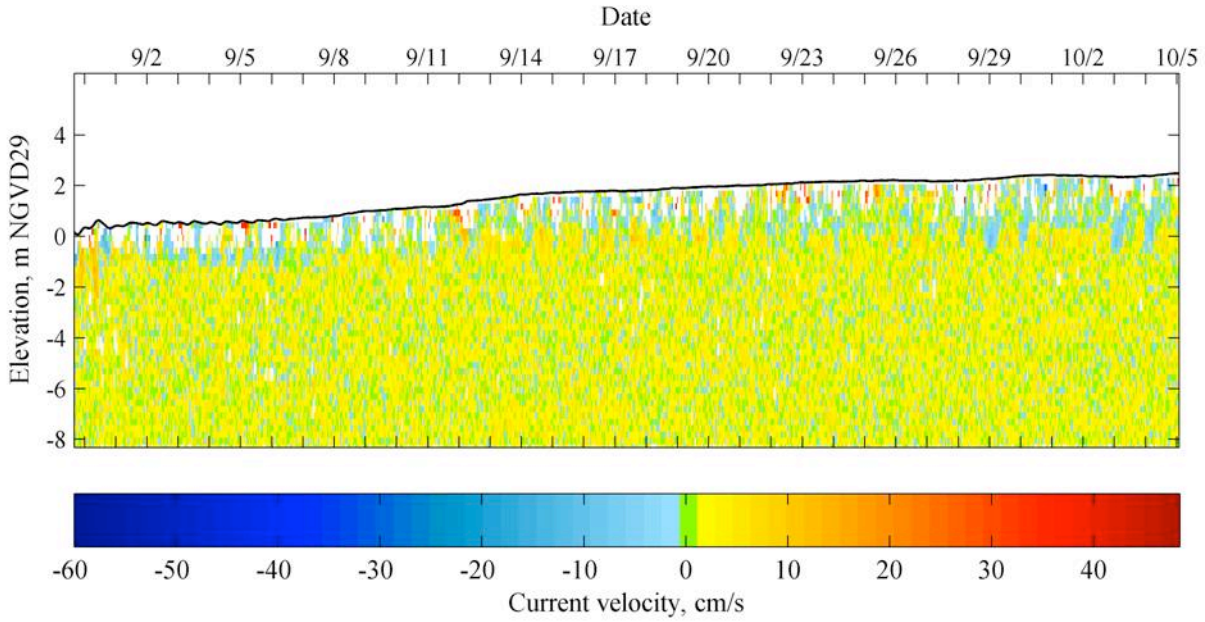

Figure 3.19. *Along-channel velocities observed at Heron Rookery during the 2009 closure. Positive flows are oriented upstream.*

Finally it is worth noting that these seiche velocities are significant (up to 25cm/s) and comparable to tidal velocities in this inner estuary. Further, the estimated volume fluxes of order 200cfs (Figure 3.18) are twice the river flow during this low-flow season. Hence, it can be expected that this wind-driven seiche is the primary source of mixing in the inner estuary and that it may control the ultimate fate of stratification during long closure events.

3.3 – Hydrographic structure

Water properties at a given location are an expression of the estuary-wide hydrographic structure, which fluctuated with tides when the mouth was open and evolved steadily through the long closure in fall 2009. Temperature and salinity are the primary physical properties as they combine to determine the density of the water, which in turn plays an important role in establishing pressure gradients due to horizontal differences in the density and thus in the weight of the overlying water (these are known as baroclinic pressure gradients, in contrast to barotropic pressure gradients that are due to horizontal differences in water elevation and thus in the weight of overlying water).

All water properties are subject to the same patterns of transport and mixing, circulating cooler saline seawater and warmer freshwater through the estuary. However, the mass balances that control the evolution of properties also include non-conservative terms (such as the surface warming of water) that differ between properties. Thus salinity patterns do not match temperature, nutrient or dissolved oxygen patterns and one may find habitats with any combination of property values. As there is neither source nor sink for salt dissolved in estuarine waters, salinity is a conservative property and provides the clearest view of transport and mixing patterns in the estuary. However, the distribution of temperature, nutrient, or dissolved oxygen in the estuary is not simply explained by the mixing of freshwater with seawater (as is true for salinity), thus an explanation of distributions also requires knowledge of the spatial pattern in processes such surface heating, respiration, and photosynthesis.

3.3.1 – Spatial distribution of salinity

The distribution of salt in the Russian River estuary is comprised of vertical and longitudinal structures. The longitudinal structure is due to seawater mixing in from the mouth while freshwater flows in at the landward boundary. The vertical structure is due to the large density difference between seawater and freshwater, so that saltier waters flow landward beneath seaward flowing low-salinity waters (see plots in Behrens & Largier 2010).

For convenience, one may identify 3 hydrographic zones in the Russian River estuary: (i) the outer estuary, up to Sheephouse Creek, is characterized by strong tidal currents and associated fluctuations in salinity; (ii) the mid-estuary, from Sheephouse Creek to Heron Rookery, is characterized by weaker and more variable tidal fluctuations in salinity and the trapping of saline water in deeper pools for extended periods of time; and (iii) the inner estuary, landward of Heron Rookery, is often completely fresh, but saline waters intrude under specific tidal conditions or during closure events and pockets of salinity may be retained in deep pools following such an event.

Vertical structure in salinity is strong in the Russian River estuary. While the water column may mix during strong tidal flows, the continual inflow of river water ensures that stratification is rapidly re-established as currents weaken hours later or as ebb-tide straining helps to counter vertical mixing. During neap tides, or as the mouth constricts tidal flows, vertical stratification will persist unbroken, even at stations near the mouth. The wind may also deform or mix the surface freshwater layer as surface stress is imposed directly on this thin low-salinity layer – but, as for the tide, as soon as the wind weakens, near-surface stratification is re-established.

During tidal periods, currents may be strong enough in the outer estuary to mix the whole water column during spring flood tides, but stratification can be observed during neap tides and during ebb tide flows (even during spring tides). During ebb tides, the drag of the bottom strains the water column, slowing deeper waters and allowing lower salinity waters to move over them near-surface. In the mid-estuary, tidal currents are weaker and the longitudinal salinity gradient increases so that a clear salt wedge structure can be seen – advancing landward on flood tides and retreating seaward on ebb tides. In the mid/inner estuary, intrusions of this salt wedge will fill deeper sections and form a trapped lower salt layer that remains resident even as the tidal flow of freshwater moves back-and-forth over it. These trapped saline layers are specifically noticeable as the tide range decreases, which occurs as the mouth shoals and begins to close.

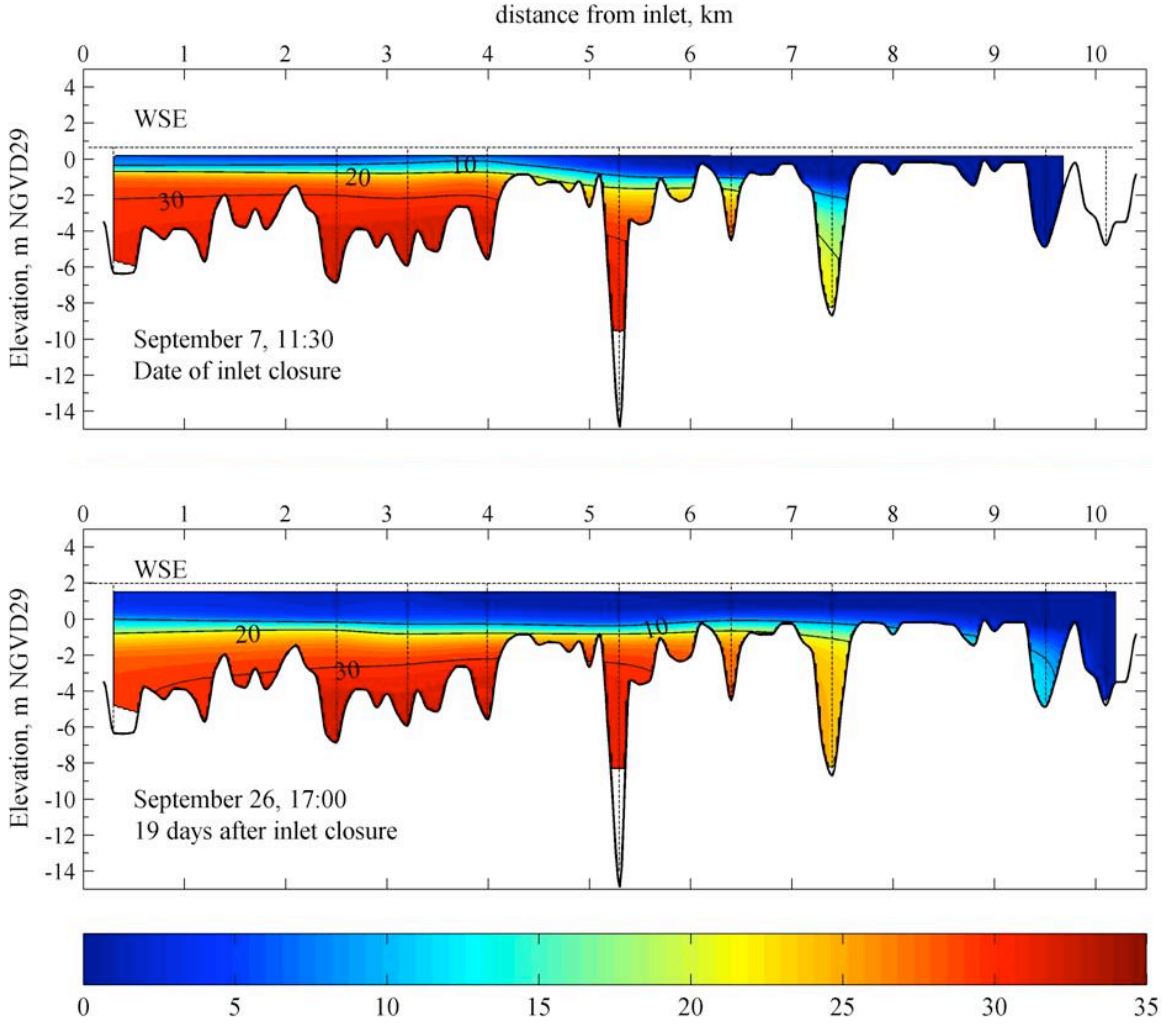

Figure 3.20. *Salinity distribution during the September closure event. Units are psu.*

3.3.2 – Salt intrusion into inner estuary

In addition to establishing estuarine habitat, the intrusion of saline waters into the inner estuary may pose a problem for water extraction. Figure 3.21 provides a record of salinity at mid-depth at Heron Rookery (mid-estuary) and Freezeout Creek (inner estuary). Clearly tidal range plays a strong role in the upstream transport of salt. Salinity increases at Heron Rookery during spring tides (and decreases during neap tides), with saline waters making brief appearances during spring tides in May and June and remaining resident in July and August, even before the mouth closed. However, following closure, salinity at Heron Rookery increased suddenly from about 13 to 17 psu and then increased again to about 20 psu. In the absence of tides, the diurnal wind seiche is critical as it will also tilt the pycnocline and may allow intrusions of saline water to move over shoals between deeper sections. A further increase to 24 psu occurred following a wave overwash event in mid-September.

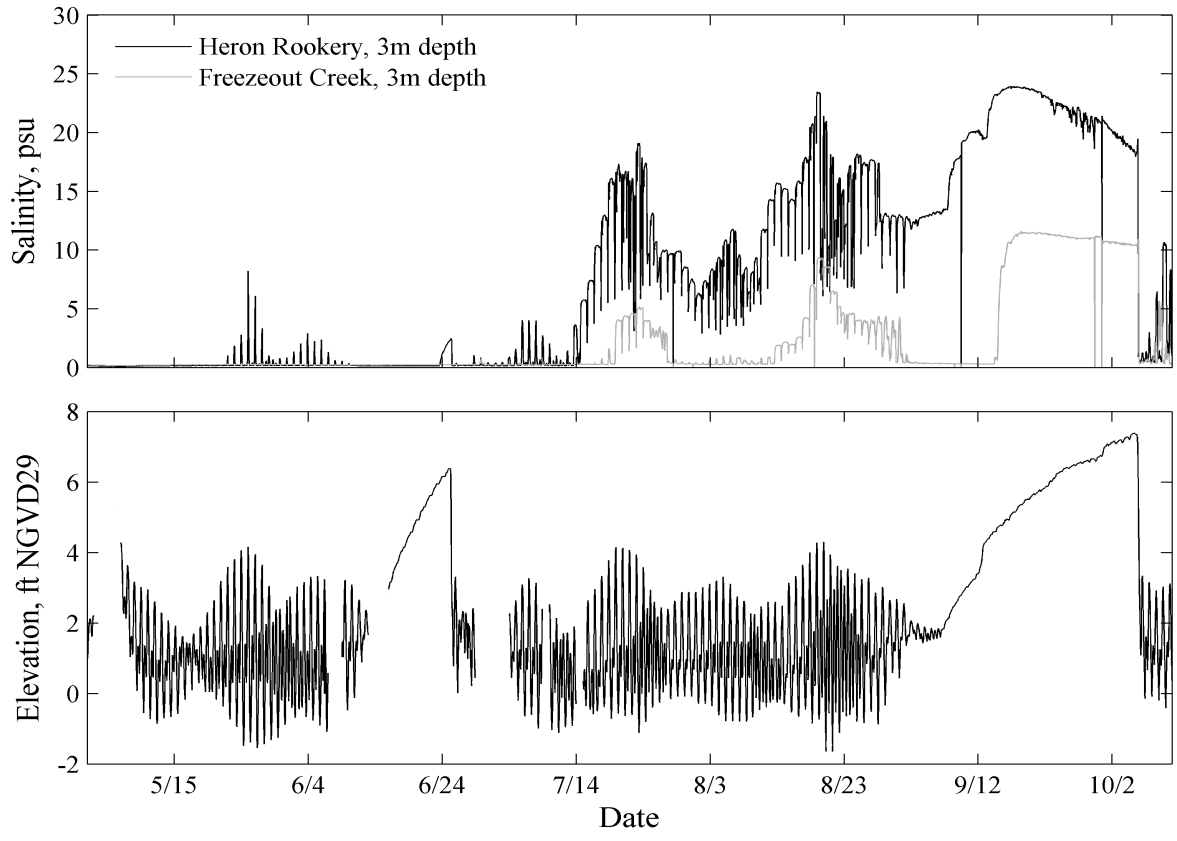

Figure 3.21. *Mid-depth salinity at Heron Rookery and Freezeout Creek (top panel) and water level at Jenner (bottom panel) during 2009.*

Saline waters are also observed at mid-depth at the Freezeout Creek station, intruding here during spring tides and lower river flows in July and August (but not in May/June), and during closure following the noted wave overwash event (Figure 3.21). The salinity at Freezeout Creek is always less than at Heron Rookery and persists for shorter periods during tidal periods. The delay in the appearance in salinity at Freezeout with respect to Heron Rookery indicates that the saline layer must first be established (filled up) at Heron Rookery before the saline waters can intrude further. No time-series data are available for locations further upstream (e.g., deeper sections at Moscow Road bridge and Cassini pool).

The use of mid-depth data offers an incomplete view as saline waters may intrude earlier and sink to the bottom in the deep pools at Heron Rookery and Freezeout Creek. Depending on where surface waters connect with groundwater, even a thin bottom layer could pose a problem for water extraction from shallow near-bank wells. It is suggested that near-bottom sondes continue to be included in future monitoring. Further, the record of salinity from a mid-depth sonde suspended from a surface buoy will be influenced by changes at mid-depth as well as changes in the depth of the sonde relative to the pycnocline as a result of changes in surface elevation (e.g., the brief spikes towards higher salinity at Heron Rookery prior to mid-July may be due to intrusions or due to tidal lowering of the sonde across a sharp non-tidal pycnocline; likewise, the brief spikes towards lower salinity at Heron Rookery after mid-July may be due to tidal raising of the sonde across the same non-tidal pycnocline – an effect also seen in late September, perhaps due to the wind-driven seiche during closure).

3.3.3 – Spatial distribution of temperature

The distribution of heat in the estuary (represented by temperature) is explained by the mixing of seawater and freshwater, as described above for salinity, plus the flux of heat across the air-water interface. Any exchange of heat between water and estuary bottom is considered negligible. Temperature is important as a component of density (which in turn drives currents) and as a determinant of habitat for juvenile steelhead and other estuarine biota. As thermal patterns are mostly dominated by tides and mirror salinity patterns when the mouth is open, attention here is directed at thermal patterns during the September-October closure event.

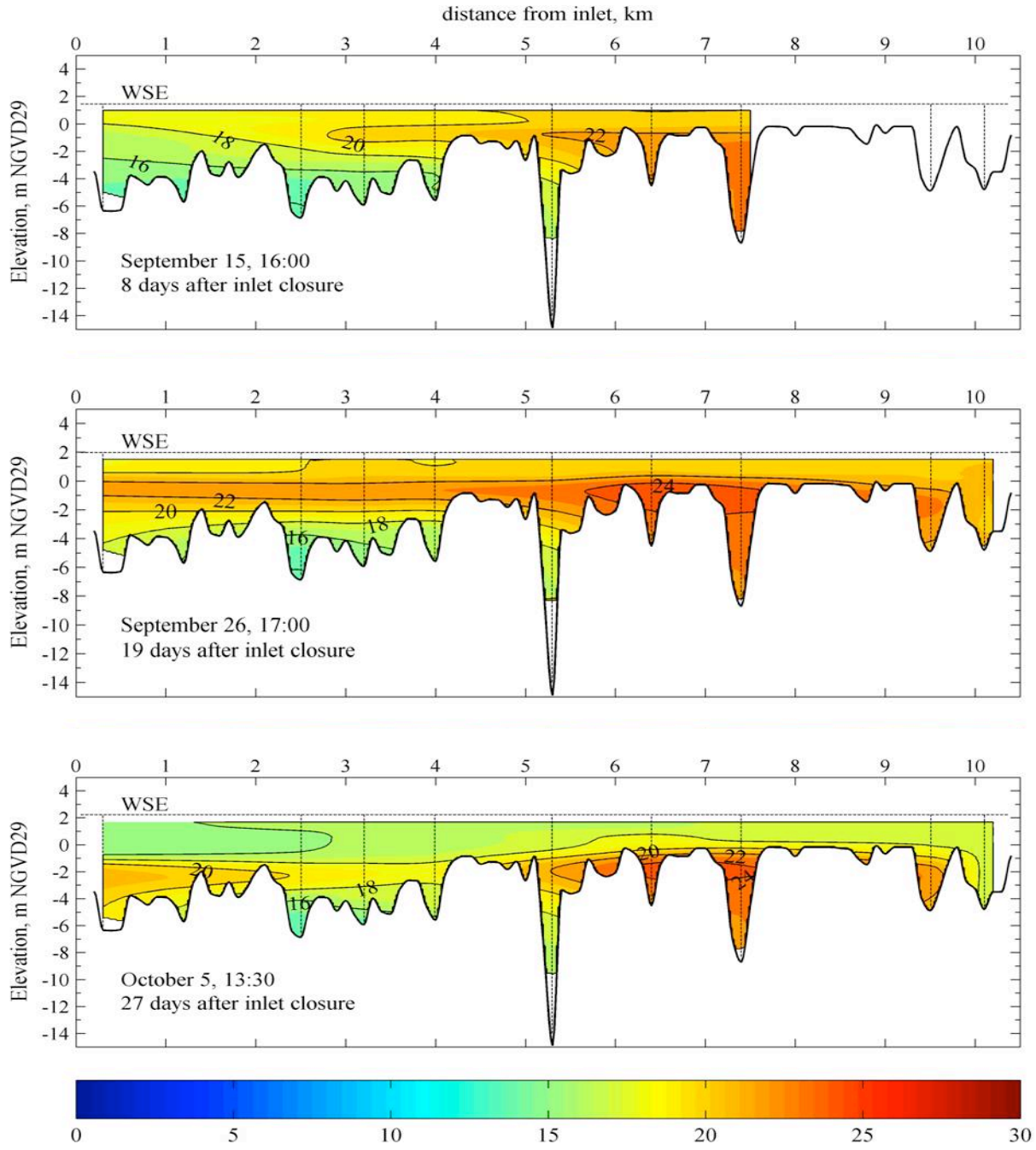

Figure 3.22. *Water temperatures during the September closure event. Units are ^{o}C.*

In general, a 3-layer thermal structure is observed, with cool deep waters, warm waters at mid-depth and moderate temperatures near-surface (Figure 3.22). The water at depth in the outer estuary is primarily seawater that has been trapped below a pycnocline. The strength of the estuary pycnocline precludes any mixing across it and these deep waters are fully insulated from warming of surface waters – thus they remain cool for weeks.

Immediately above these waters, in the pycnocline is a layer that neither mixes with underlying cool waters nor near-surface waters, but it is near enough to the surface to receive heat in the form of radiation (which can penetrate a few meters of water). These mid-depth waters warm significantly to well over 20°C. While near-surface waters are warmed more strongly by radiation, they also lose heat through evaporation and by direct contact with the cool sea and nighttime air and do not warm above 20°C (except well upstream) and show seasonal cooling in October. Wind mixes this cooling effect over the uppermost 2m.

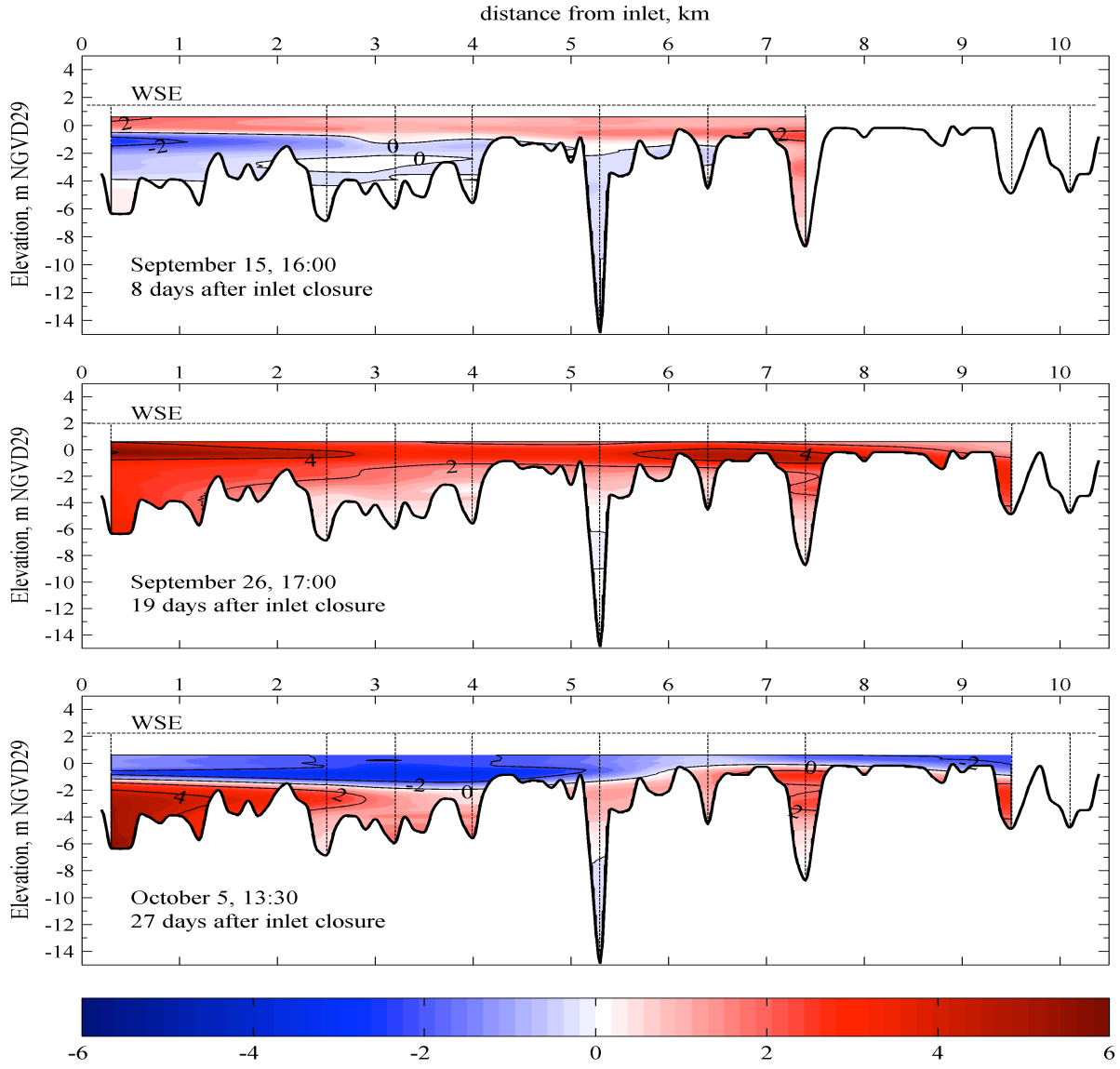

Figure 3.23. *Change in temperature from September 7. Units are °C.*

On closer inspection, one can see that the deepest waters also warm during the closure event, specifically near the mouth (Figure 3.23). This may be due to deeper penetration of thermal radiation, due to slow vertical mixing of warmer waters from the lower pycnocline, or due to horizontal mixing with warmer waters at depth further from the mouth. Given the strong winds near the mouth, one may expect stronger vertical mixing here than elsewhere. Alternatively, the homogenization of deep-water temperatures may be driven by weak seiche-induced effects at depth and this would account for the strongest warming in the location where the initial temperatures were lowest (i.e., the mouth). Also of interest in Figure 3.23 is the cooling of mid-depth and deeper waters in the first week, which was due to intrusion of a mass of cold salty water imported via wave overwash between 12 and 14 September.

3.3.4 – Spatial distribution of dissolved oxygen

The distribution of dissolved oxygen (DO) in the estuary is explained by a combination of air-sea oxygen flux and uptake or release of oxygen through in-water biological and chemical processes (including processes at the sediment-water interface). Oxygen is important as a determinant of habitat for juvenile steelhead and other estuarine biota.

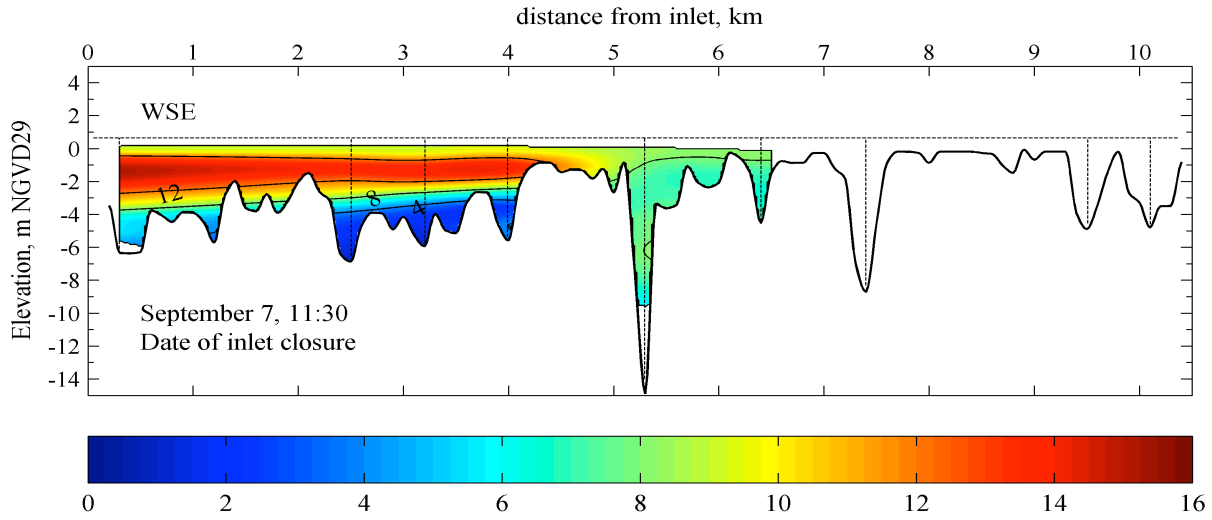

Figure 3.24. *Dissolved oxygen on September 7, 2009. Units are mg/L.*

In general, surface waters are well oxygenated by exchange with the atmosphere and low levels of oxygen are only observed due to respiration beneath the pycnocline, which isolates the lower layers from the oxygenated upper layers. However, while the estuary is tidal the lower layer is comprised of seawater that has been recently imported to the

estuary, along with its full complement of dissolved oxygen (~8mg/L), so that hypoxia is not seen in the outer estuary. However, where saline water is trapped in deeper sections of the mid/inner estuary and remains resident for a week or more, the oxygen in the water can be used up and low levels are observed in this trapped lower layer. Further, as the tide is increasingly muted prior to the closure on 7 September, dense saline waters are also trapped in the deeper sections of the outer estuary, so that hypoxic waters are observed in the lower layer at Paddy's Rock and Bridgehaven before the mouth closes completely (Figure 3.24).

During closure, one sees 3 layers: well-oxygenated surface layer, de-oxygenated bottom layer, and a super-saturated layer at mid-depth. Light easily penetrates down to these mid-depth waters trapped in the pycnocline and the resulting photosynthesis releases large amounts of oxygen during daylight hours. Given that these waters neither mix with underlying hypoxic waters nor overlying surface waters, this excess dissolved oxygen cannot escape. However, at night photosynthesis stops and respiration continues, reducing DO levels at this depth – mid-depth SCWA sondes show DO levels decreasing 4-5mg/L overnight.

The depth of light penetration and photosynthesis is shown in Figure 3.25 – a plot of photosynthetically active radiation (PAR). The one-percent light level has been shown to be a strong indicator of the limiting depth for photosynthesis (e.g. Dennison *et al.* 1993, O'Donahue *et al.* 1997). Figure 3.25 shows this limiting depth for September 26. Comparing Figure 3.25 with oxygen distributions on the same day (Figure 3.27) shows that the depth of the one-percent light level approximates the upper boundary of the hypoxic region.

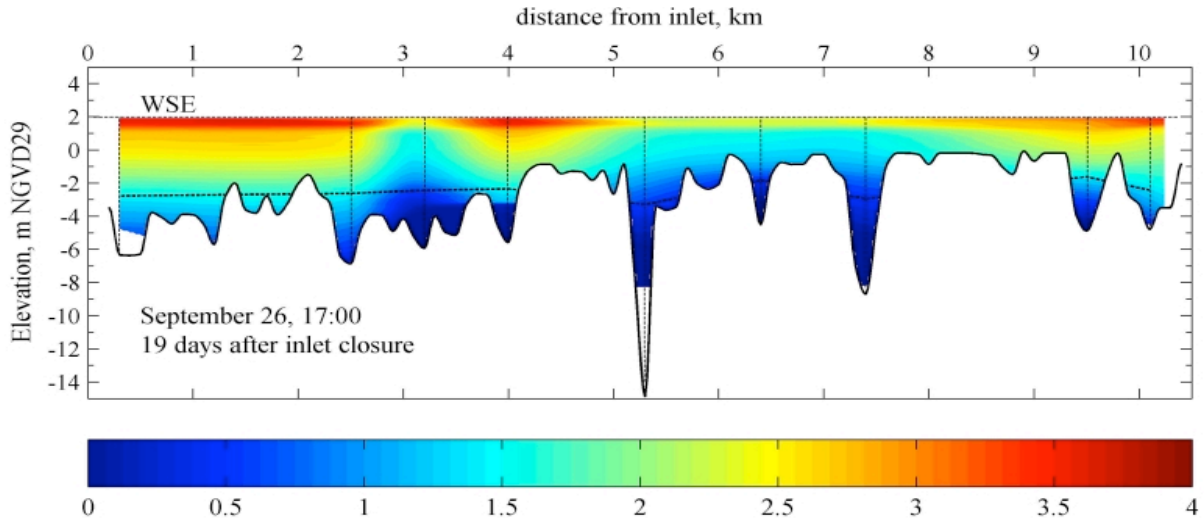

Figure 3.25. *Log PAR (irradiance) values on September 26 – the dashed line indicates the one-percent light depth.*

Preliminary biochemical oxygen demand (BOD) measurements in the Russian River estuary were obtained by Tamminga and Largier (2009) and found to be consistent with drawdown of DO levels over the course of a week. In Figure 3.26, data from near-bottom sondes maintained by SCWA prior to 2009 were plotted as a function of time (i.e., time since bottom water was trapped at depth and isolated from re-oxygenation). Typical uptake rates reduce DO from 8mg/L in about a week. However, in most cases near-bottom anoxia is delayed or prevented, presumably by the penetration of some light to drive photosynthesis in these deeper waters.

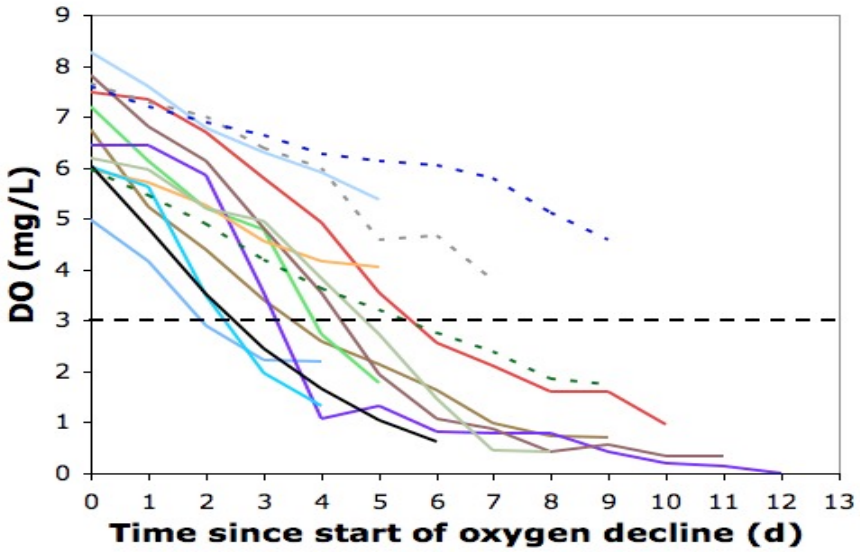

Figure 3.26. *Daily average levels of dissolved oxygen for events monitored by SCWA oxygen sondes during closure events prior to 2009 (Tamminga & Largier 2009).*

While near-bottom waters at Paddy's Rock (and nearby pools like Bridgehaven) were already hypoxic by the time of closure (following several days of drawdown while trapped during muted tides), the remainder of the mid/outer estuary was oxygenated at the time of closure (Figure 3.24). However, with the formation of a trapped layer of dense saline water throughout the estuary, near-bottom DO levels decreased so that hypoxia was observed at depth throughout the mid/outer estuary within a week of closure. While DO profile data from the inner estuary is lacking, it is expected that hypoxic conditions developed within a week of the trapping of a saline lower layer at Heron Rookery and Freezeout Creek (as described in section 3.3.2 above) – this is seen in SCWA sonde data. This hypoxia is evident at Heron Rookery on 26 September, persisting through the remainder of the closure period (Figure 3.27).

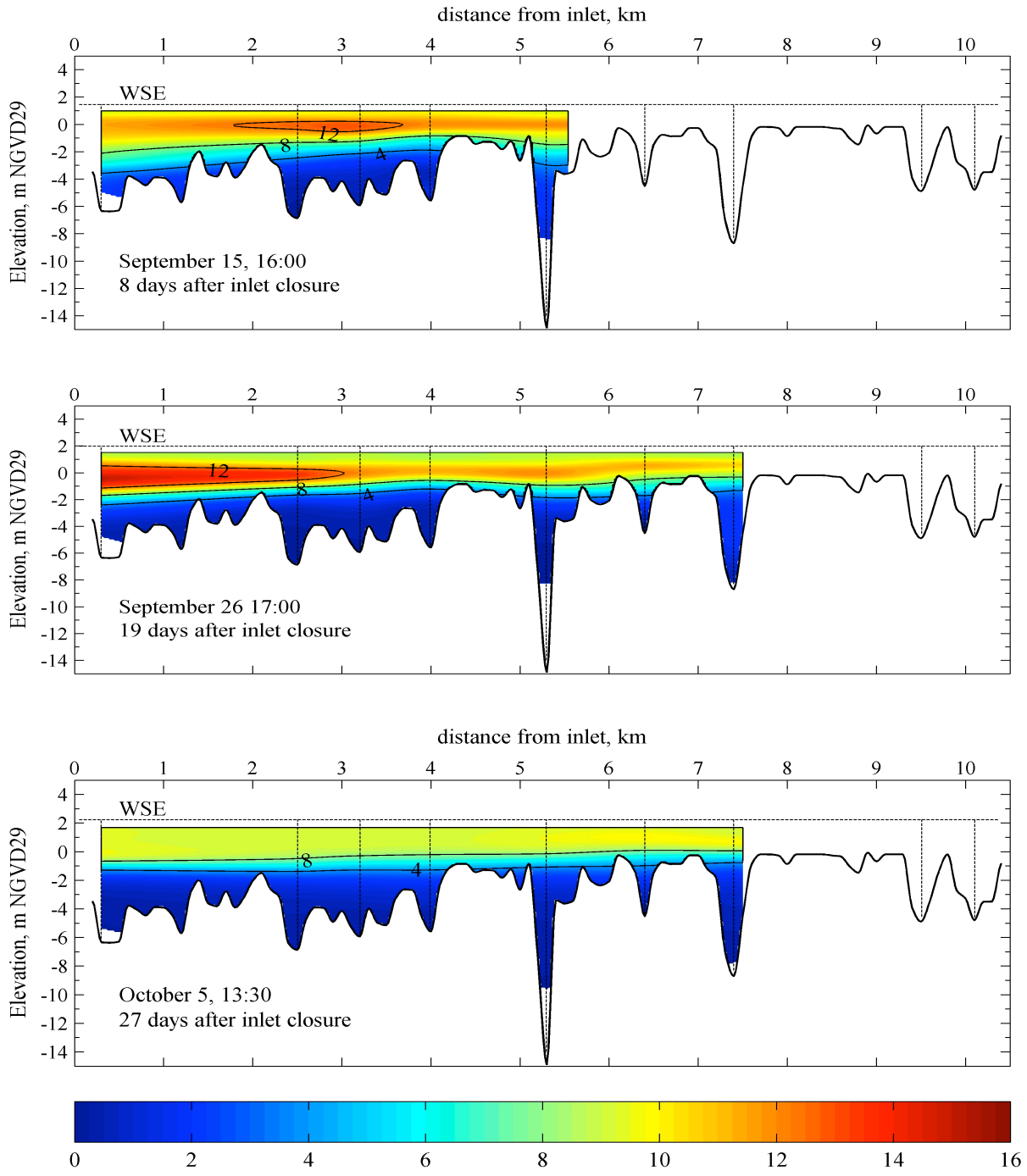

Figure 3.27. *Dissolved oxygen during the September closure event. Units are mg/L.*

3.4 – Stratification and water-column stability

From the above discussion of DO, temperature and salinity fields in the estuary, it is clear that stratification plays a primary role in circulation, water residence and water properties during closure events. Stratification controls vertical mixing, reducing it or completely suppressing it, and results in observations of deep-water hypoxia, mid-water hyper-oxic conditions and mid-water hyper-thermal conditions. Stratification is also evident during open-mouth periods, most notably during neap tides and weaker river flow. Density of the water during closure (Figure 3.28) shows a vertical difference of about 20kg/m^3 and sharp stratification approaching 10kg/m^4 throughout the mid/outer estuary. During high-tide conditions (Figure 3.28), the water column at the mouth is well mixed while the outer estuary is partially mixed, with stronger stratification observed in mid-estuary.

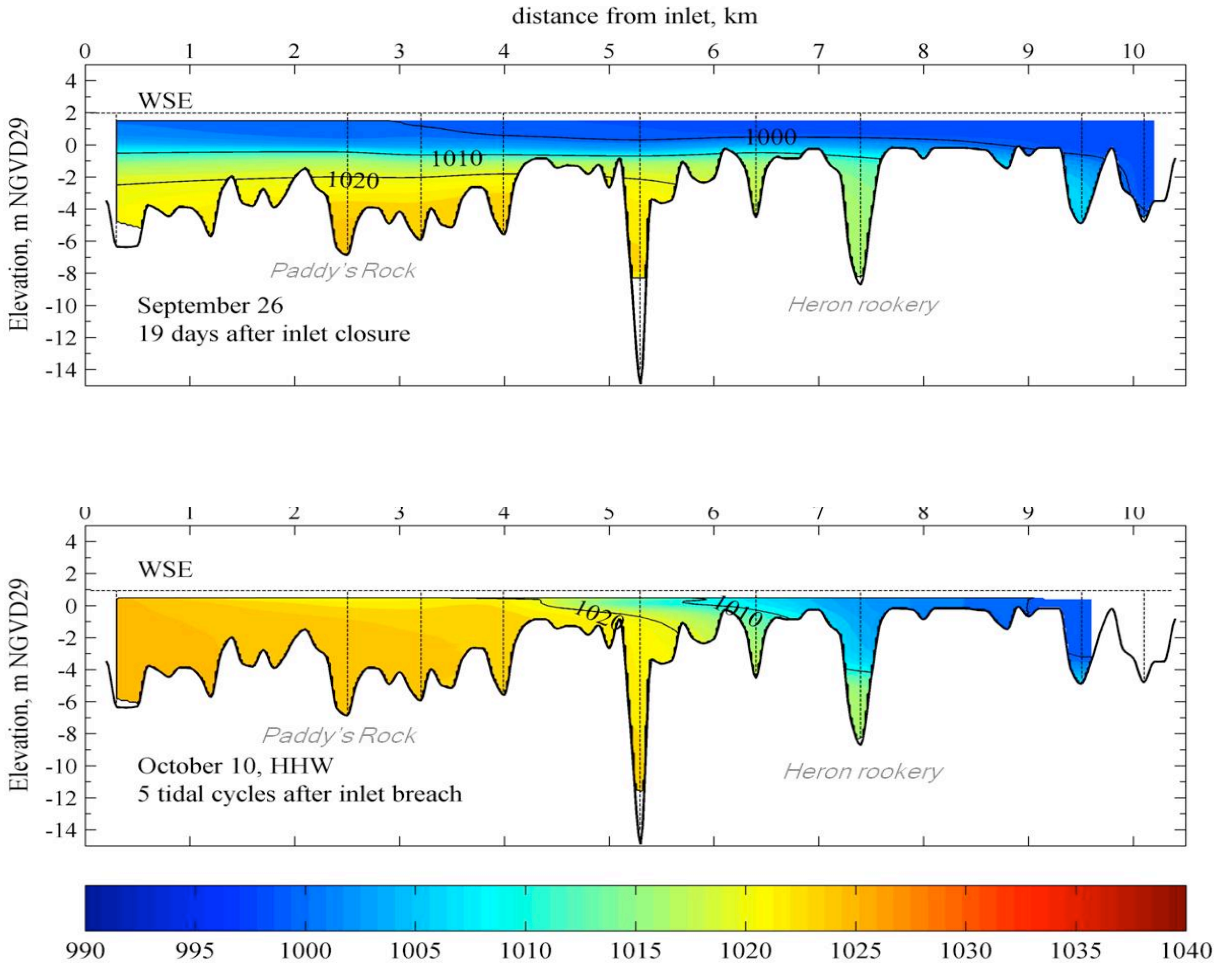

Figure 3.28. *Density during closure (top) and high tide (bottom). Units are kg/m^3.*

The strength of stratification is assessed through its resistance to mixing. This is typically done through an analysis of the likelihood that current shear will be strong enough to overcome the stability due to density differences (i.e., Richardson Number calculations), or by estimating the amount of energy needed to mix a water column completely irrespective of how it is done (i.e., the potential energy anomaly, or stability). The first approach resolves vertical differences, identifying mixing layers and pycnocline layers across which there is no mixing. The second approach takes a bulk approach and considers the entire water column. Both approaches confirm that the strong stratification in the Russian River is unlikely to breakdown during closure periods.

3.4.1 – Richardson Number – assessing stability as a function of depth

The gradient Richardson number *Ri* is used to investigate stability as a function of depth (Fischer *et al* 1979):

$$Ri = N^2 / (\partial u/\partial z)^2 \qquad \text{[Eq. 7]}$$

where $N^2 = -g\,(\partial\rho/\partial z) / \rho_0$ is the buoyancy frequency (or Brunt-Väisälä frequency), g is gravity, ρ is density, u is current speed, and z is depth, and ρ_0 is depth-averaged density. The denominator is the shear frequency, and represents the generation of kinetic energy, which may overcome the potential energy associated with buoyancy and mix the local part of the water column. Thus, by combining these two parameters as the gradient Richardson Number one obtains a comparison between the tendencies for mixing and stratification. For values below 0.25, turbulent kinetic energy tends to grow (increased mixing), whereas above this value turbulence decays (e.g. Friedrichs *et al.* 2000; Simpson *et al.* 2005; Monismith, 2009).

The gradient Richardson Number can only be calculated where one has profiles of both velocity and density, as is available from Heron Rookery from the bottom-mounted ADCP and boat-based CTD. Three scenarios are examined here: (1) the transition from a constricted to a fully closed inlet, (2) a fully closed inlet and (3) an open inlet with full tidal conveyance.

On the day of closure (7 September), a strong pycnocline ($\partial\rho/\partial z \sim 5\text{kg/m}^4$) is observed between -1 and -3m NGVD (Figure 3.29). In the 2m-layer above the thermocline $Ri <$ 0.25 and mixing is active. Below -1m NGVD, weak currents cannot overcome strong stratification and $Ri >> 0.25$ indicate the stability of this pycnocline layer. Well below the pycnocline density gradients are weak, but recorded velocities are within the ADCP error range and *Ri* estimates are unreliable.

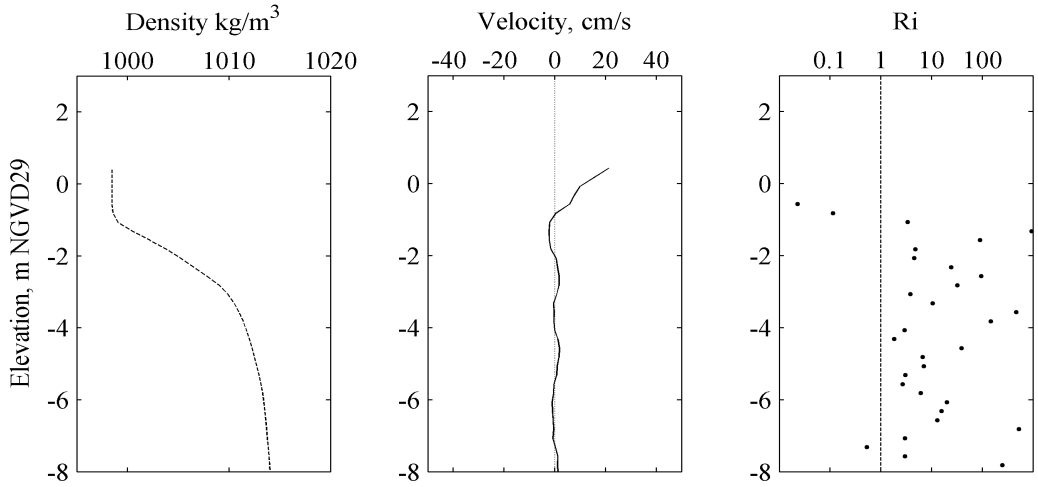

Figure 3.29. *Profiles of density, velocity, and Ri at Heron Rookery on 7 September.*

By 30 September, three weeks after closure, the pycnocline was sharper ($\partial\rho/\partial z \sim 10$ kg/m^4) and the density of the lower water column had increased owing to the intrusion of more saline waters (Figure 3.30). Surface wind stress maintains a 2m-thick mixed surface layer ($Ri < 0.25$), but high Ri is observed in the pycnocline, in spite of shear associated with the wind-driven return flow (described in section 3.2.3).

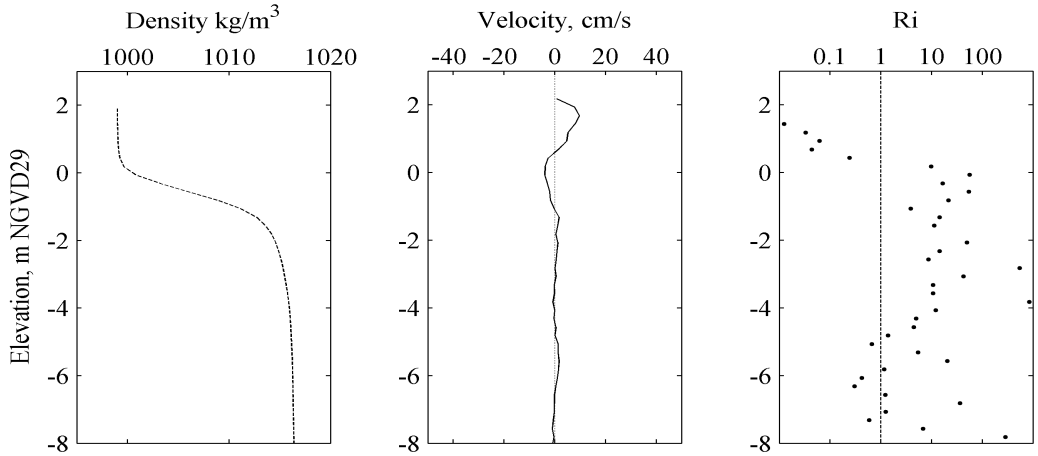

Figure 3.30. *Profiles of density, velocity, and Ri at Heron Rookery on 30 September.*

The October 5 breach of the inlet and associated increases in river and tidal flows resulted in a significant export of salt. On 6 October, the pycnocline is 3.5m lower, but

still strong, due to continued trapping of high-salinity water at depth (Figure 3.31). *Ri* remains low in the surface mixed layer, down to -2m NGVD, but increases below that due to stratification in the upper pycnocline.

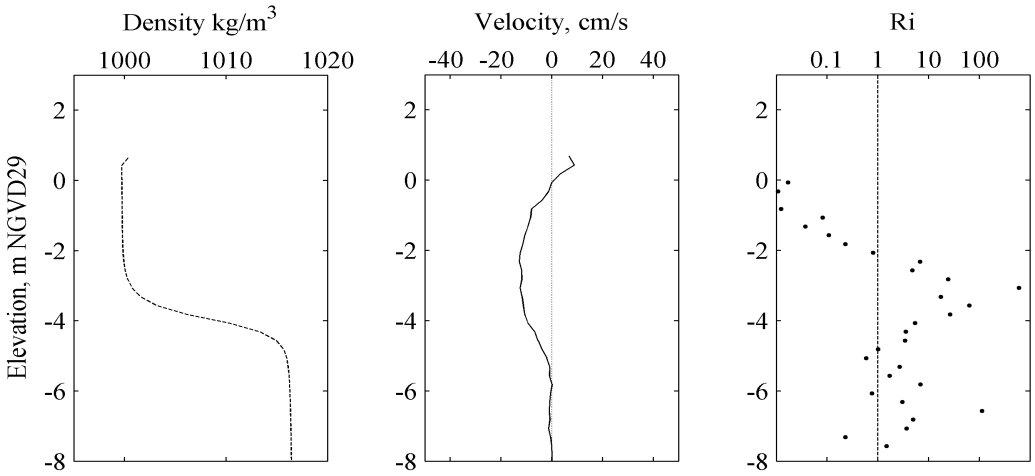

Figure 3.31. *Profiles of density, velocity, and Ri at Heron Rookery on 6 October.*

Where continuous vertical profiles of density or velocity are not available, one can calculate the bulk Richardson Number from top-bottom differences in current speed and water density:

$$Ri_{\Delta} = \Delta\rho \; g \; h \; / \; \rho_0 \; U^2 \qquad \text{[Eq. 8]}$$

where $\Delta\rho$ is the surface-bottom difference in density, h is the depth of the water column, and U is the vertically-averaged flow velocity – and the critical value is taken as 1. Hourly density data are available from sondes deployed at the bottom, middle, and top of the water column at Paddy's Rock, and at the bottom and two mid-depth locations at Heron Rookery. Hourly velocity data are available from ADCPs at these sites. Ri_{Δ} estimates were made at Heron Rookery only when the surface was known to be fresh, on the basis of surface salinity observed at Sheephouse Creek. This approach allows a time-series of Richardson Number estimates, although it does not resolve differences over depth.

The Paddy's Rock time-series confirms that the water column was stratified during the entire June-July 2009 period, despite spring-neap variations in tidal amplitude and river inflows that varied from 70-140 cfs (Figure 3.32). While Ri_{Δ} never approached 1, it does vary strongly with the tide, changing by two orders of magnitude, most noticeably as

diurnal variations during the spring tides in mid-July. Although velocity data are not available at the mouth, the observation of an isopycnal water column at the mouth (e.g., Figure 3.28) suggests that indeed Ri_Δ would decrease below 1 at that station.

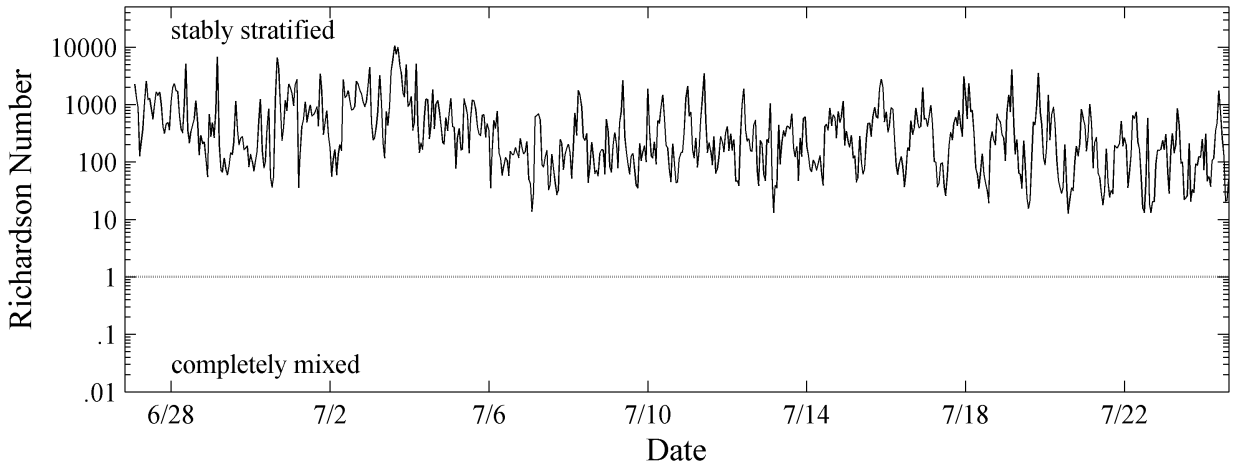

Figure 3.32. *Time-series of bulk Richardson Number Ri_Δ at Paddy's Rock during July 2009. Dashed line indicates $Ri_\Delta = 1$.*

The Heron Rookery time series shows the tendency for mixing during inlet breach events (Figure 3.33). At all other times, Ri_Δ is well over 100 (in contrast to Paddy's Rock). Weak diurnal fluctuations in Ri_Δ are observed during the September closure events, a response to wind-driven seiche.

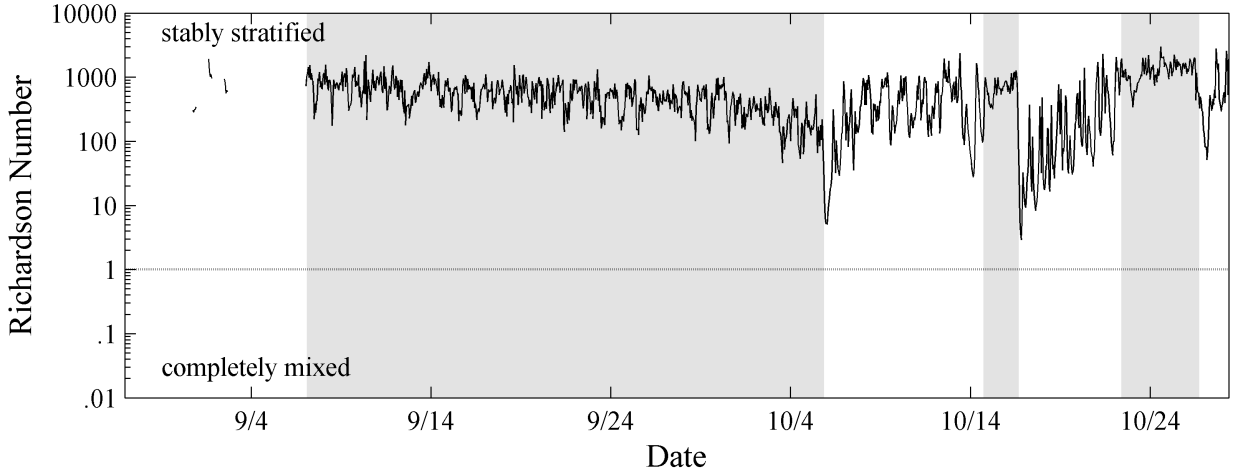

Figure 3.33. *Time-series of bulk Richardson Number Ri_Δ at Heron Rookery during September-October 2009. Dashed line indicates $Ri_\Delta = 1$.*

3.4.2 – Assessing water column stability – the potential energy anomaly

The second method for assessing stratification is to assess the stability of the entire water column by estimating the amount of energy needed to mix it completely, irrespective of how this may be done. Simpson & Bowden (1981) and Simpson *et al.* (1990) defined the "potential energy anomaly" as a measure of the excess buoyancy present in the water column, which represents a potential energy deficit compared with a mixed water column. Alternatively, it is the amount of mixing energy required to bring about a fully mixed (isopycnal) density profile. The potential energy anomaly ϕ is defined as:

$$\phi = \frac{1}{h}\int_{-h}^{0}(\rho_{mean} - \rho)gzdz \qquad \text{[Eq. 9]}$$

where $$\rho_{mean} = \frac{1}{h}\int_{-h}^{0}\rho(z)dz \qquad \text{[Eq. 10]}$$

A higher ϕ value implies a more stable water column, i.e., more energy needed to mix the water column. Two scenarios are sketched in Figure 3.34: vertical density profiles during strong mixing (e.g. tidal conditions) and weak mixing (e.g. constricted inlet, stratified estuary) scenarios.

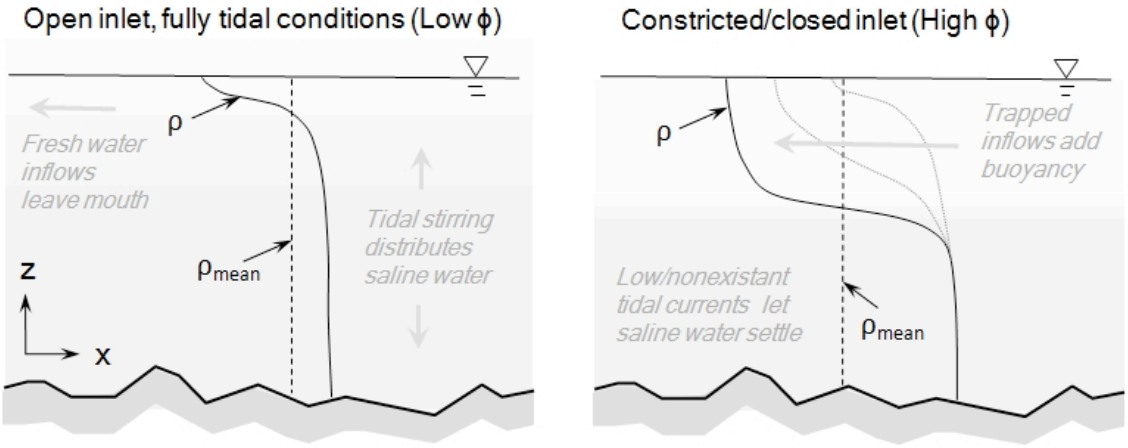

Figure 3.34. *Idealized representations of density profiles during conditions with strong mixing (low ϕ) and weak mixing (high ϕ).*

Using CTD profiles of $\rho(z)$, time-series of stability are calculated for each station (Figure 3.35). The water column at the Mouth station is least stable, showing zero stability at times (when already mixed, i.e. isopycnal). Stability at Paddy's Rock and Bridgehaven is also low during tidal conditions, approaching zero at times. Mid/inner estuary stations exhibit significant stability even during tidal conditions due to the salt water trapped at depth in these deep sections (e.g., Sheephouse Creek). The stable lower layer at these stations may develop hypoxia, even when the mouth is open. When the mouth is open the innermost stations are entirely fresh and exhibit near-zero stability (Figure 3.35).

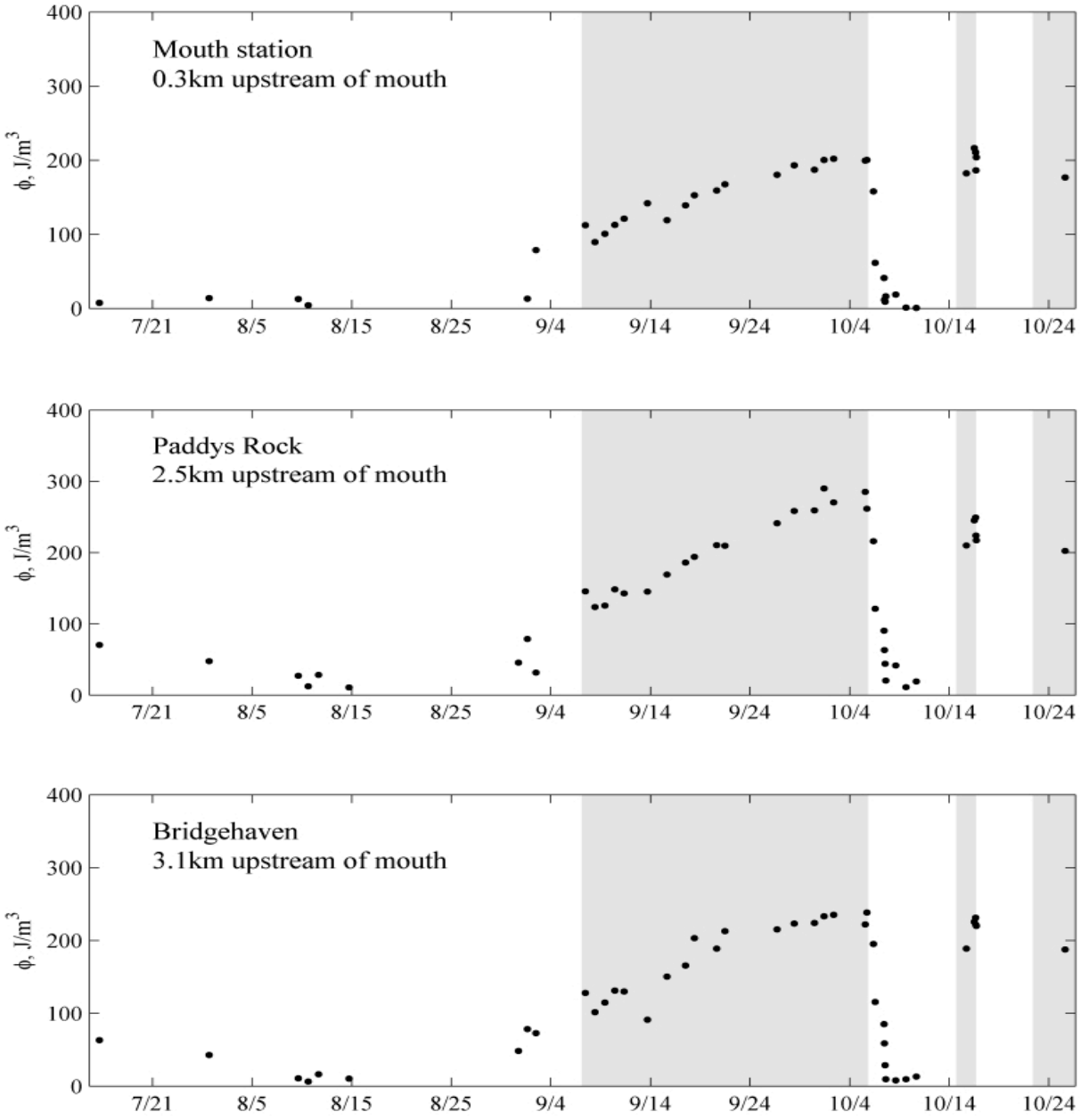

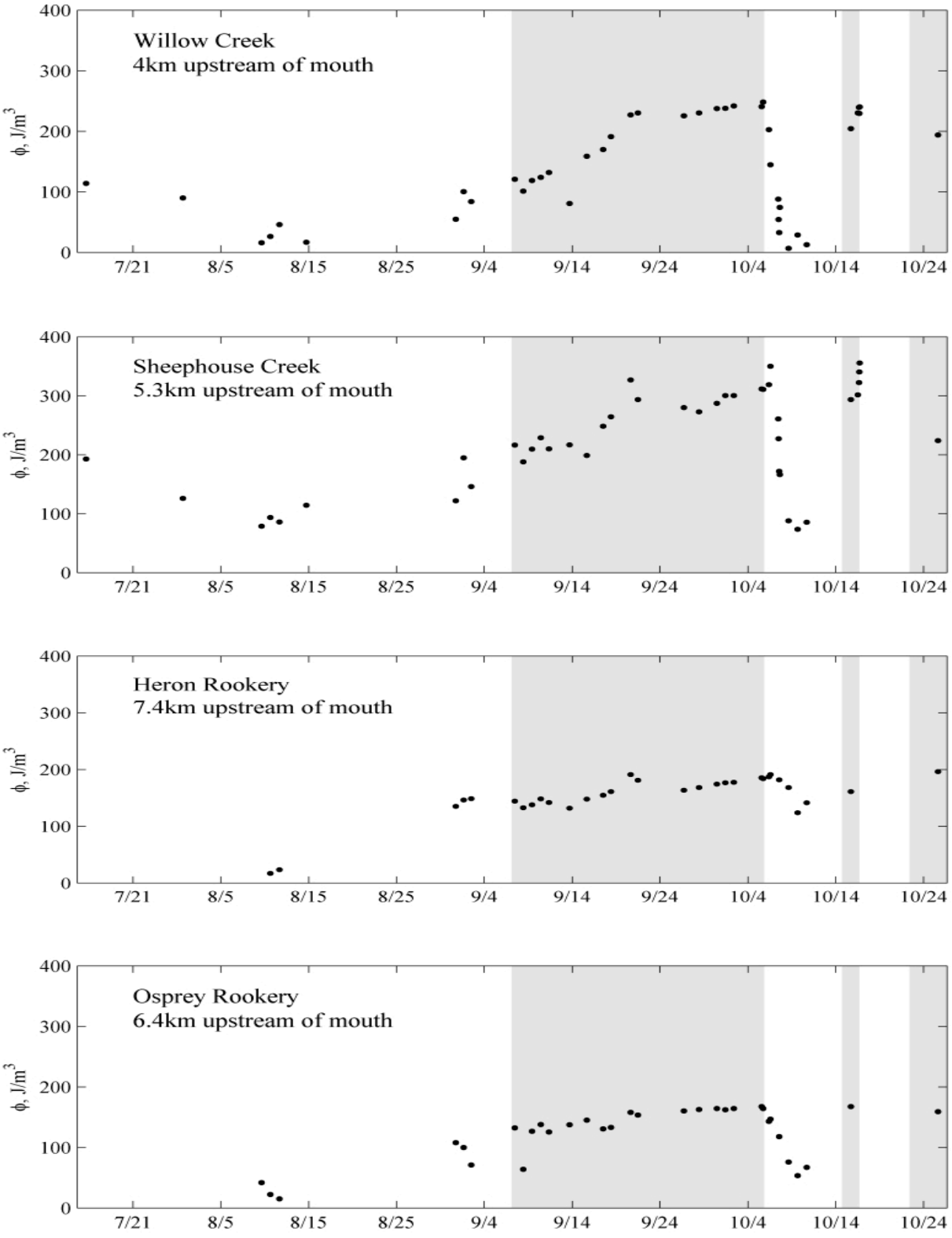
Willow Creek
4km upstream of mouth
Sheephouse Creek
5.3km upstream of mouth
Heron Rookery
7.4km upstream of mouth
Osprey Rookery
6.4km upstream of mouth
ϕ, J/m3
0
100
200
300
400
7/21
8/5
8/15
8/25
9/4
9/14
9/24
10/4
10/14
10/24

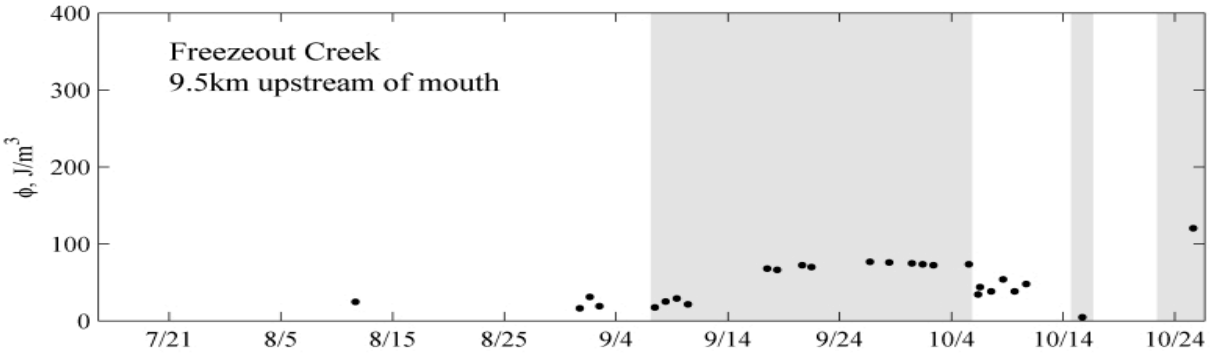

Figure 3.35. *Time-series of potential energy anomaly ϕ at primary stations.*

During the muted tidal conditions, prior to closure on September 7, an increase in water column stability was observed at all stations as stratification built up. This happened in spite of a net loss of salt from the estuary over this week (see Section 3.5), evidently due to the outflow of freshwater near-surface which resulted in lower surface salinities and increased stability throughout the estuary. Velocity data show a near-surface (freshwater) jet extending only 20-30 cm into the water column (see Figure 8.3 in Behrens & Largier 2010), which could account for the advective export of salt from this uppermost layer and the consequent sharpening of the pycnocline (and higher water column stability).

During the September-October closure event, water column stability continued to increase for all stations, due to increasing water depth as well as the intrusion of saline waters near-bottom at inner estuary stations and the intrusion of low-salinity waters near-surface at outer estuary stations. The increase in stability at the Mouth station is least, and levels out after about 3 weeks. This is due to the slow decrease in the salinity of deeper waters (Figure 3.36), countering the increase in ϕ due to increasing h. In contrast, near-bottom salinity at Paddy's Rock remains unchanged below 5m NGVD, and little changed at all depths below 3m – the height of the shoal separating this station from the Mouth station (cf., Largier & Taljaard 1991, Largier & Slinger 1991). Whether due to vertical mixing or seepage through the bar, the changing vertical distribution of salinity near the Mouth station may have led to a decrease in stability if the mouth remained closed longer – and, ultimately, the stability may reduce enough for the water column to be mixed by winds. This could flush out the lower-layer hypoxia and the possibility of this happening needs further attention.

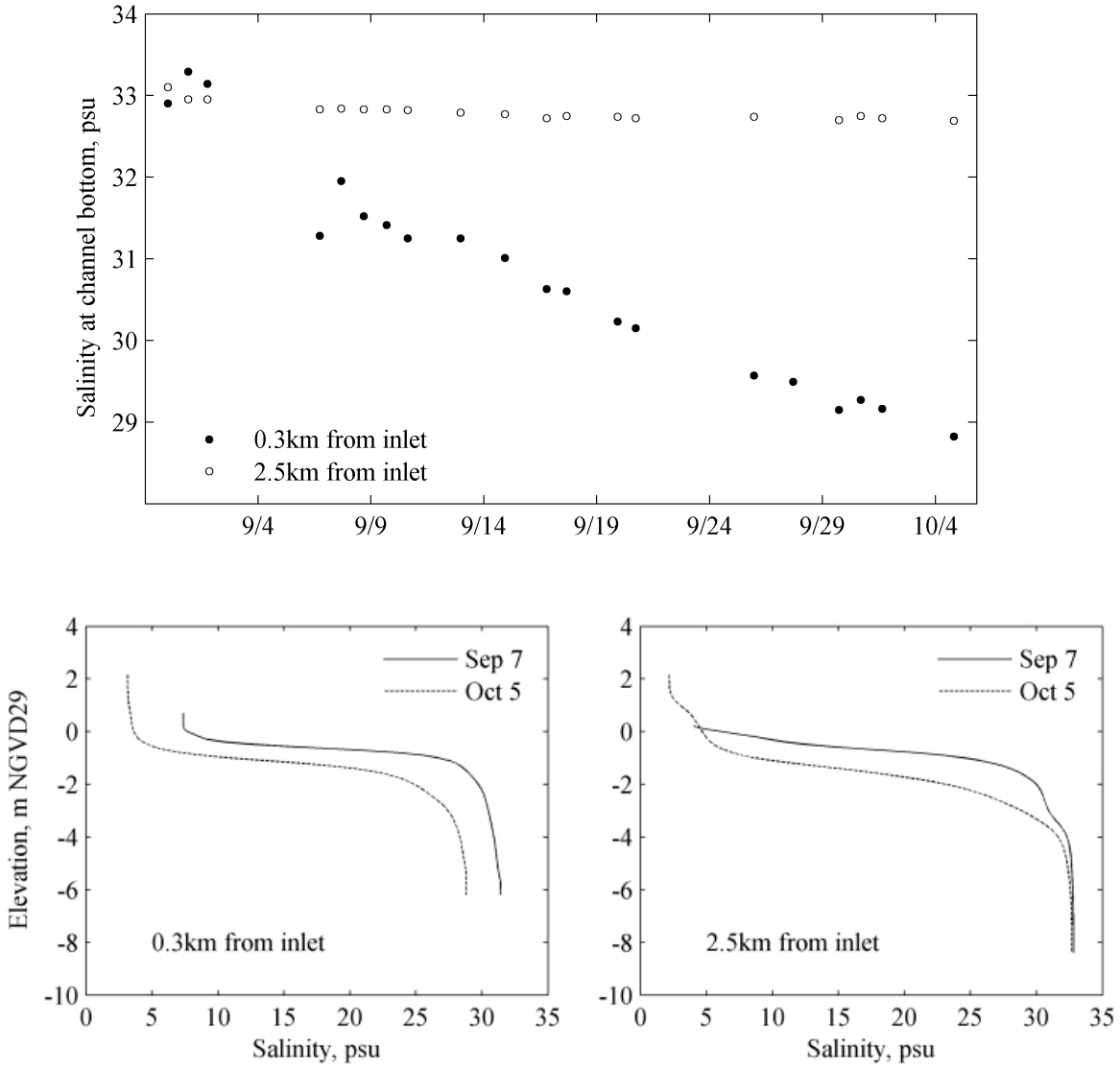

***Figure 3.36**. Decreasing bottom salinity at Mouth station in contrast to steady bottom salinity at Paddy's Rock station (top panel), and vertical profiles of salinity at start and end of closure period for stations at Mouth (0.3km) and Paddy's Rock (2.5km).*

After the October 5 breach event, stability of the water column went to zero for the stations seaward of Sheephouse Creek, consistent with mixing of the water column in the outer estuary. However, at stations that retained a dense layer at depth, e.g., Sheephouse Creek, stability dropped but remained significant. Despite flows over 0.6m/s at Heron Rookery, the lower water column was unaffected by these flows and dense waters remained trapped there.

During the late-October closure, stability at Freezeout Creek was higher than previously observed as a result of a higher salt mass in the estuary. This was probably due to a large wave event at the time of closure. Following closure, this salt mass intrudes landward, introducing more sub-pycnocline to Freezeout Creek and thus enhanced stability.

3.5 – Salt and oxygen mass budgets

3.5.1 – Salt budget for estuary

Given that salt is neither created nor destroyed on the time scale of interest in this study, the total mass of salt contained in the estuary is conserved in the absence of inflows or outflows of saline water. It is unaffected by processes, such as river inflow, evaporation, mixing, or density-driven exchange flows. Thus one can learn much about the estuary by tracking the salt mass. A gain of salt implies a gain of saline water (i.e., seawater) and a loss of salt implies a loss of saline waters from the estuary. Of specific interest is the possible loss of estuary water via seepage through the sand barrier, as addressed through a water budget (Section 3.1).

To calculate the mass of salt from CTD profile data, the estuary was divided into segments (Figure 3.37), and each segment was divided into incremental volumes in the vertical direction. These incremental volumes were multiplied by CTD measurements of salinity at corresponding depths and summed up over the total depth to obtain a salt mass for each segment for each time a CTD profile was obtained. The total mass of salt in the estuary is obtained from a sum of all segments. For this analysis, the upper boundary is taken as Freezeout Creek, since the upstream pool at Moscow Bridge received only negligible amounts of salt during the monitoring period.

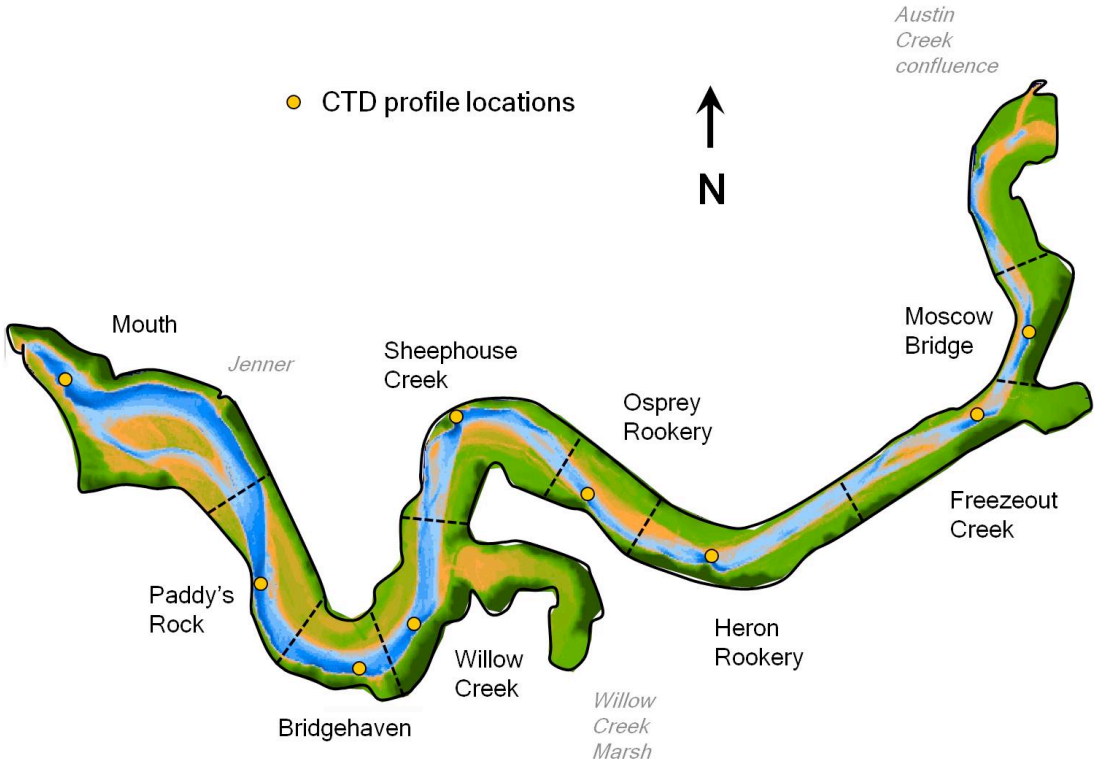

Figure 3.37. *Estuary bathymetry from 10m x 10m grid. Segments used for salt balance calculations and associated CTD station locations are shown.*

The change in salinity during the September-October closure is shown Figure 3.38. In general the outer estuary loses salt and the inner estuary gains salt, resulting from the baroclinic forcing that moves excess salt from near the mouth and redistributes it so that isopycnals are level. The pivot point between decrease and increase in salinity is 5 km from the mouth, over a long shallow ridge between Willow Creek and Sheephouse Creek. The depth of strongest change is near the pycnocline depth, so that much of the observed change may be due to relaxation of the tilt in the halocline after closure. The increase in salinity observed in the outer estuary on 15 September is presumably a result of the wave overwash event between 12 and 14 September, with some of the intruding seawater mixing into the pycnocline and spreading landward at this depth.

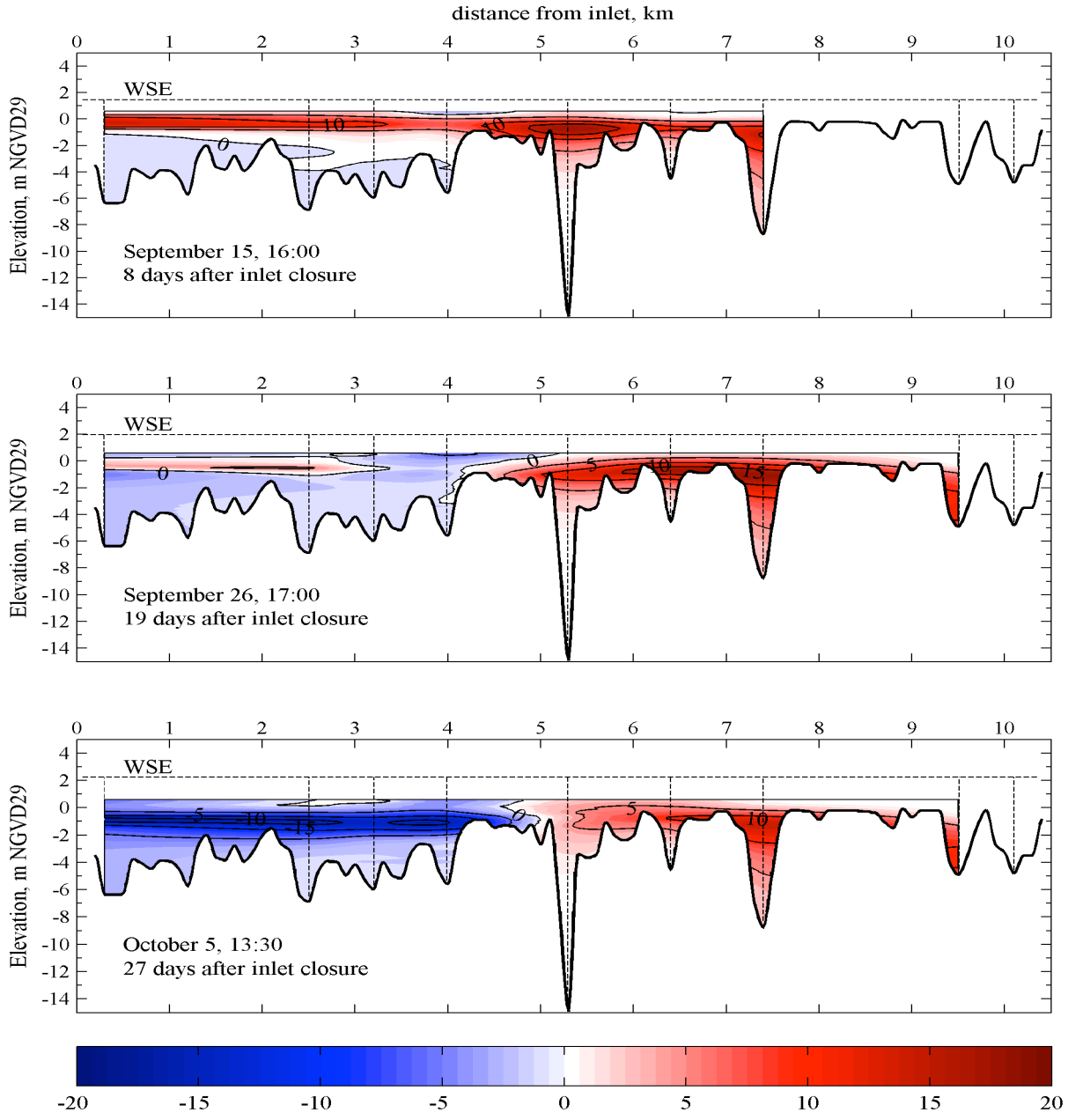

Figure 3.38. *Change in salinity from September 7. Units are psu.*

Also of interest is that the loss of bottom salinity is strongest near the mouth (vs Paddy's Rock) – indeed the salinity is lower here than at Paddy's Rock or Bridgehaven (see Figure 3.20) and it is warmer (Figure 3.22). This may reflect a local loss of saline waters as seepage through the sand barrier (and replacement by warmer, fresher overlying

water) or it may reflect vertical mixing, which is expected to be strongest due to strong winds near the mouth. This phenomenon deserves more attention.

The export of saline waters from the estuary is confirmed by the time-series of total salt mass (Figure 3.39). Following an initial increase of about 10^7kg of salt due to the wave overwash event (12-14 September), the total mass decreased at about 10^7kg per week. In Figure 3.39 one sees that the outer estuary experienced a steady decrease in salt, while salt in the inner estuary continued to increase slowly due to ongoing intrusion of saline waters there. While some salt may be lost to groundwater aquifers, it is expected that this loss be primarily due to a flux of estuary waters through the sand barrier.

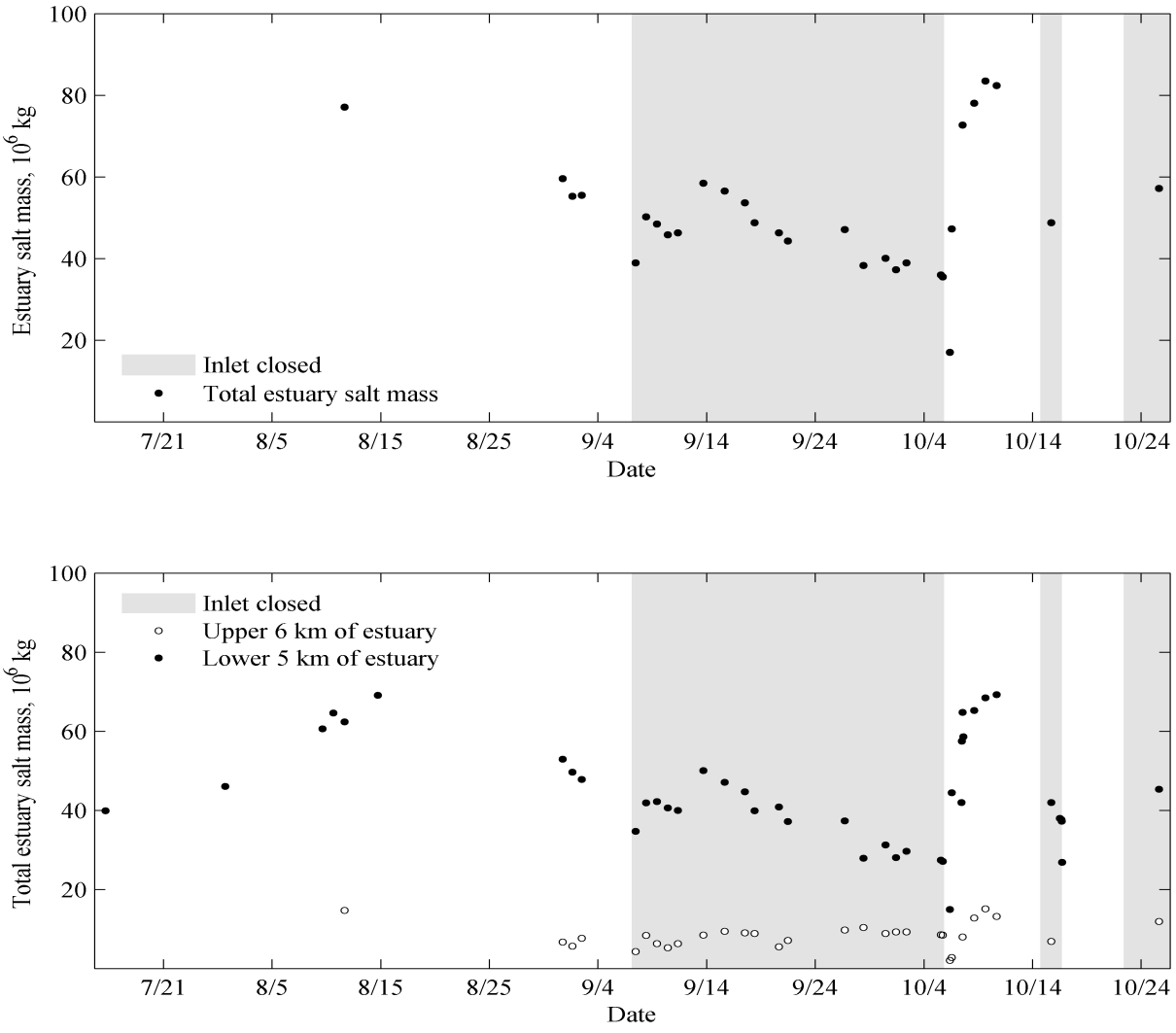

Figure 3.39. *Time-series of salt mass for entire estuary (top panel) and for inner and outer portions of the estuary (lower panel).*

Further, it is expected that this flux is likely to be stronger near-surface owing to the narrower berm at this height and thus shorter travel distances (see Equation 3 in section 3.1.3). Alternatively, the outflux of estuary waters may be strongest at a preferred depth, as suggested by the results shown in Figure 3.6 (e.g., a high-conductivity route through the rip-rap underlying the jetty). Either way, the dominant flux is likely to be above 0ft NGVD and comprised primarily of water with salinity less than 10psu (see Figure 3.20). Indeed if one simply compares the ratio of salt lost and water lost over common periods between wave-overwash events, one obtains an average salinity of 12.4kg/m^3 ~ 12.4psu. While this may include some high-salinity bottom water, it is clear that the majority of water and salt is lost from above the pycnocline. Analyses for specific periods are listed in Table 3.1 – one can see that the salinity of water lost is decreasing, presumably due to the increased water level and increased potential for berm throughflow above the height of the pycnocline, which remains relatively constant (Figure 3.20).

Table 3.1. *Salinity of flows leaving the estuary between wave overwash events.*

Time period	Starting salt mass (10^6 kg)	Ending salt mass (10^6 kg)	Average flow rate (cfs)	Export salinity[1] (ppt)
9/8 - 9/11	50.2	46.3	28.1	18.9
9/15 - 9/21	56.5	44.3	56.5	14.7
9/27-10/5	47.0	36.0	58.8	9.6

[1] Calculated by dividing change in salt mass by total flow loss during period

During high river flow, the mouth is open and much of the salt is flushed from the estuary, e.g., on 6 October, following breaching (and even lower in winter). In the absence of high flows, total estuary salt mass varies markedly with tide range and inlet state. There are also tidal fluctuations that are not shown here as all CTD surveys were conducted close to high tide. After the flushing of salt in the October 5 breach event, salt mass increased with each subsequent tidal cycle.

Salt masses during the two later closure events are comparable to that during the extended closure event. However, the initial salt mass at the time of closure may vary, resulting in different conditions during closure with more or less saline water to re-distribute and more or less stability due to differences in the salinity and thickness of the lower layer. In particular, the stability of the waters near the mouth are important as there is a possibility that stratification may be broken down there if initial stability is weaker (see discussion of possible decreasing mouth stability in section 4.3.2).

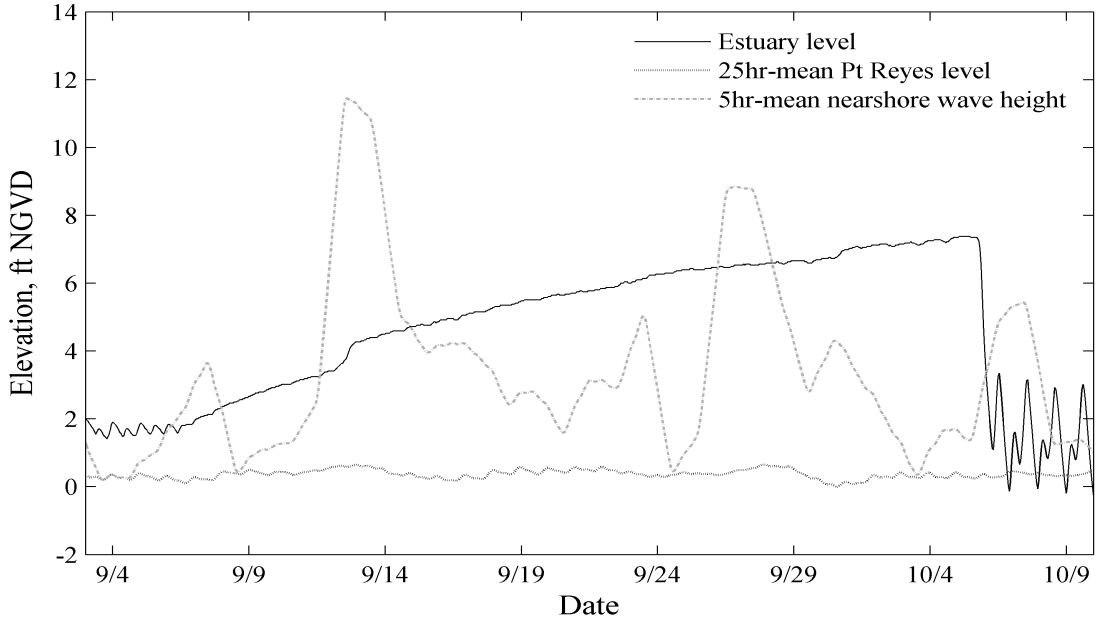

Figure 3.40. *Nearshore wave height, estuary water level and ocean sea level during September closure event.*

The initial mass of salt trapped in the closed estuary depends on the tidal and river conditions at the time of closure, e.g., if the mouth is closed on a spring high tide and/or during low flows then one expects a larger mass of salt. Equally important are wave events during closure or as overwash events following closure. Because wave overwash is a one-way flux, a significant mass of salt can be pumped into the estuary during a single event. Three large-wave events occurred during the closure period, between 7 September and 5 October (Figure 3.40). It appears that wave overwash occurred each time, although the 12-14 September is clearly the largest event. Following each wave event, water level rose and temperature declined. There are few prior studies or even references to this phenomenon. However, the contribution of these events to water and salt budgets (and maybe also DO and nutrient budgets) may be quantified from information on beach characteristics (e.g., berm width, face slope, and height) combined with wave statistics. These data are not available for 2009.

3.5.2 – Preliminary dissolved oxygen budget for estuary

To better understand the spatial distribution of dissolved oxygen as described in Section 3.3.4, a budget analysis can be constructed for DO as done above for salt. Primary

interest is in a budget that explains the sub-pycnocline occurrence of hypoxic and anoxic conditions. Further, due to DO data quality problems in the mid/inner estuary, the oxygen budget only includes the portion of the estuary downstream of Sheephouse Creek. The majority of the estuary volume (and specifically the vast majority of hypoxic volume) is contained within this region. Additionally, the oxygen budget is only calculated for waters below the elevation of the water surface on the date of closure (7 September).

As described in Section 3.3, the sub-pycnocline waters are trapped for the entire closure event and thus DO levels will only be affected by respiration, photosynthesis and any mixing that may occur. Below the 1-percent light level, there is a net respiration of organic matter (i.e., net uptake of oxygen) and DO declined during the closure period (although typically attaining minimum values within about a week). However, there is an upstream progression in de-oxygenation that reflects the intrusion into the inner estuary of near-bottom, dense, saline waters (Figure 3.27). As the salt wedge spread upstream due to baroclinic circulation and seiche-driven currents, so did the stable density interface between fresh and salty water, which precluded downward mixing of oxygenated surface waters. Ultimately, hypoxia was observed in deep waters (i.e., below 1-percent light level) across the entire estuary.

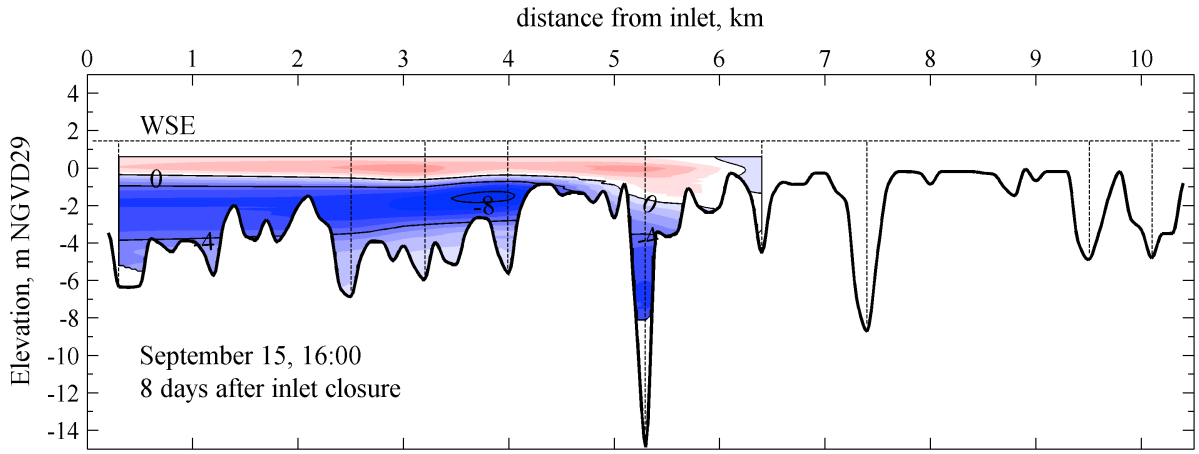

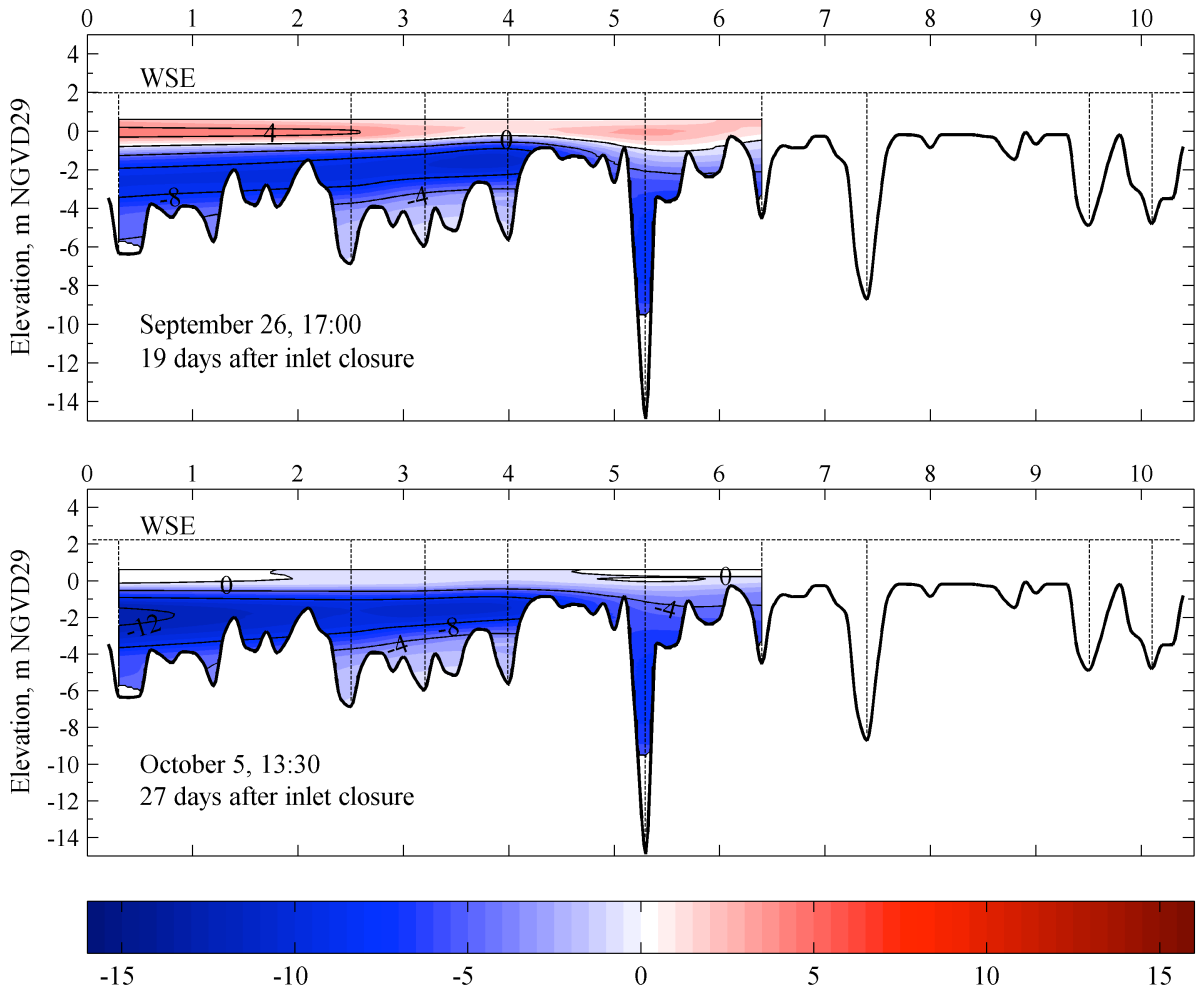

Figure 3.41. *Change in dissolved oxygen from 7 September. Units are mg/L.*

The change in DO (Figure 3.41) was calculated in the same way as for salt (Figure 3.38), by directly obtaining the difference between observed values and values observed on 7 September. Further, as for salt, one can calculate the total mass of oxygen dissolved in the estuary from data obtained from CTD profiles – see Figure 3.37 and associated description of how DO values are integrated over estuary volume. For the outer estuary (from Sheephouse Creek to the mouth), and below the elevation of the water level at closure, the total oxygen mass is shown in Figure 3.42. The DO mass decreased by about 40% during the closure (7 September to 5 October). A small increase in DO mass on 26 September coincides with a possible wave overwash event (Figure 3.40), but this may also be due to an error associated with tilting of the pycnocline owing to strong winds that day (see next section).

Given that the expansion of hypoxia into the inner estuary is excluded from this mass budget, it is interesting to review Figure 3.41 to see where DO is being lost. While the near-bottom waters have the lowest DO, these levels are already low at the time of closure and near-bottom changes in DO are small and occur prior to 15 September. However, at mid-depth, DO decreases are larger and this mid-depth loss of DO occurs across a layer that continues to thicken. Presumably this is due to decreasing light exposure at these elevations as the water level rises and as the days become shorter in the fall. It thus appears that this mid-depth and near-bottom hypoxia will not be mitigated by surface oxygenation nor by biochemical processes until the water column stratification is reduced and vertical mixing can replenish DO at these depths. Thus, the question of stability addressed in Section 3.4 becomes paramount to the understanding of the extent, severity and persistence of hypoxia and anoxia in the estuary.

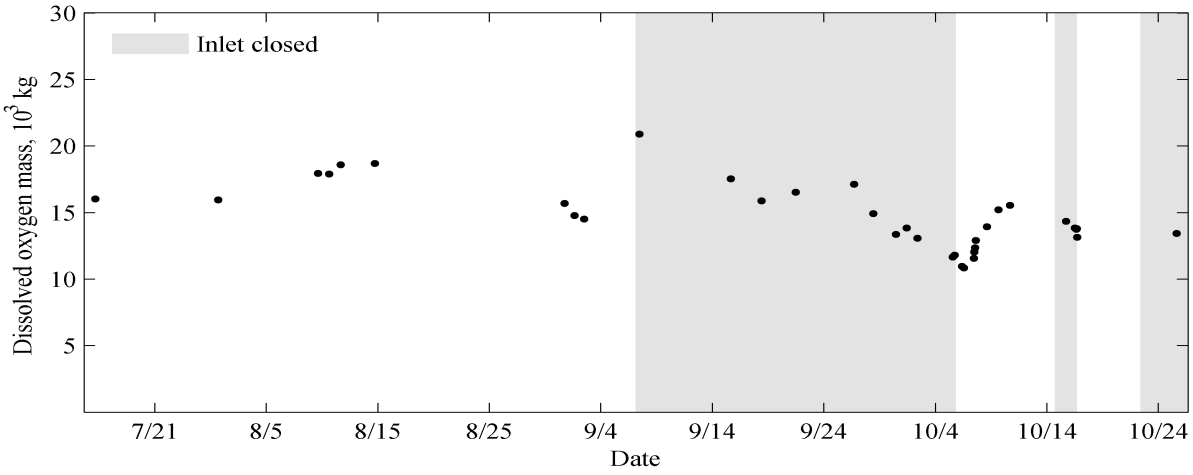

Figure 3.42. *Time-series of dissolved oxygen mass from mouth to Sheephouse Creek.*

3.5.3 – Sources of error in budgets

Calculation of salt and DO budgets include several sources of error, which are described here to provide perspective on the error in the estimates of total mass. The following factors are addressed:

- Section uniformity
- Elevation estimates
- Pycnocline tilt
- Bathymetry resolution

- Instrument precision

The error associated with each of these terms is quantified for different inlet conditions, taking a worst-case scenario (i.e., conditions that would produce the worst possible error). Thus, this error analysis does not quantify actual error but rather seeks an upper bound to the possible error in calculating salt and oxygen masses.

Section uniformity errors – The vertical distribution of salinity and dissolved oxygen in the water column is not entirely uniform throughout the estuary, even during closure. CTD profiles taken at the locations shown in Figure 2.1 may not be representative of the average vertical profile in each segment of the estuary. A fully accurate budget would require CTD profiles at many locations within each segment of the estuary, which is not feasible. The segmentation of the estuary shown in Figure 3.37 was chosen to provide reasonable accuracy while balancing time constraints. To obtain a quantitative estimate of the errors that this simplification creates, the profile in the segment was compared with the average of the profiles from the 2 adjacent segments. Tables 3.2 and 3.3 show that the total masses obtained using these average profiles differ from those from the actual CTD profiles by 1.0-8.1 percent for salt and 0.9-6.9 percent for dissolved oxygen.

Elevation estimate errors – Since water level elevations were normalized to the Jenner gage, rather than tied to known coordinates using survey equipment, reported water levels may be inaccurate by several centimeters (see discussion in Section 2). Inaccuracies in water level cause misalignments between the stage-storage curve for each segment of the estuary and the corresponding CTD profiles. Assuming that water level estimates are accurate to within ± 5cm, these errors are below 3%, regardless of inlet condition (Tables 3.2 and 3.3).

Pycnocline tilt errors – During high wind conditions, the surface of the estuary was observed to tilt by as much as 5cm in the upstream direction. A corresponding tilt (in the reverse direction) of the subsurface pycnocline is expected to be much larger and it would temporarily make the outer estuary saltier and the inner estuary fresher. Errors would arise if the tilt is non-uniform, or if the number of profiling locations is insufficient to determine its shape. The order of these errors was obtained by comparing masses estimated with a tilted pycnocline to those estimated during low-wind conditions. The maximum water surface tilt observed during CTD measurements was 2cm, which would result in a tilt of the pycnocline of about 0.8 meters (2.6 feet), estimated from the ratio between ρ and $\Delta\rho$ (Fischer *et al.* 1979). Errors for both total estuary salt and oxygen mass are below 7%, and are highest for most strongly stratified conditions (Tables 3.2 and 3.3). Most CTD measurements were taken during low wind conditions, so these results are intended to illustrate the maximum possible error observed in the data.

Bathymetry resolution errors – The resolution of the raster used to represent the bathymetry of the estuary may alter the budgets by influencing the stage-storage curve for each estuary segment. A 10m x10m raster was used as a simplification of the bathymetry data. It is difficult to assess the increase in accuracy that would be achieved by increasing this resolution, but the errors from this source are assumed to be small, since boundary cells make up a very small proportion of the estuary bathymetry even at this scale.

Instrument precision errors – CTD precision errors for salinity and dissolved oxygen measurements are very low compared to the other error sources, and are neglected.

The maximum possible error for the salt budget appears to be 13.7% and 12.5% for the oxygen budget. Actual errors are expected to be much smaller than this and to have no influence on the overall trends identified in the above sections on salt and oxygen budgets.

Table 3.2. *Error estimates for estuary salt budget*

Inlet condition, date		**Salt mass (10^6 kg)**	**Error estimates (%)**			**Total error (%)**
			Non-uniform segment conditions	± 5cm elevation error	0.8m (2.6ft) Pycnocline tilt	
Tidal	Aug 11	77	1.0	2.5	0.1	3.6
	Oct 7	73	3.4	2.3	2.4	8.1
Muted tidal	Sep 1	53	5.6	2.7	1.6	9.9
	Sep 2	55	8.1	2.7	2.9	13.7
Closed inlet	Sep 15	56	1.4	2.7	6.4	10.5
	Sep 26	47	2.7	3.0	6.9	12.6
	Oct 5	35	1.0	3.0	6.3	10.3

Table 3.3. *Error estimates for estuary dissolved oxygen budget*[1]

Inlet condition, date		Dissolved oxygen mass (10^6 kg)	Error estimates (%)			Total error (%)
			Non-uniform segment conditions	± 5cm elevation error	0.8m (2.6ft) Pycnocline tilt	
Tidal	Aug 11	18	6.9	2.6	0.1	9.6
	Oct 7	13	0.9	2.4	0.4	3.7
Muted tidal	Sep 1	14	3.2	2.7	6.6	12.5
	Sep 2	14	2.6	2.7	1.2	6.5
Closed inlet	Sep 15	18	4.1	1.8	2.0	7.9
	Sep 26	18	1.4	1.6	1.6	4.6
	Oct 5	12	1.0	1.4	6.4	8.8

[1]Dissolved oxygen budget only includes the lower 5.3km of the estuary

4. Discussion

Circulation, stratification, and water properties were monitored in the Russian River estuary during late summer and fall 2009 – a dry year in which river flow was managed at a lower level than normal. Specific attention is directed at conditions during a month-long closure event in September-October. A dense lower layer of high-salinity water is trapped in the estuary when the mouth closes, with water column stability increasing over time as well as an expansion of stable stratification into the inner estuary, which is devoid of salt during periods of higher river flow. Within a week of strong stratification being established, the near-bottom waters become hypoxic (i.e., below the 1-percent light level). At mid-depth, however, penetration of light leads to photosynthesis and a stable layer in which oxygen levels are super-saturated during the day. At similar depths, thermal radiation is also trapped and water temperatures are maximum. A thin surface layer is typically well mixed and in equilibrium with the atmosphere in terms of both dissolved oxygen and temperature. Stratification and deep-water hypoxia persist until tidal action returns with opening of the mouth in October.

While dense waters may be trapped beneath a pycnocline even during times when the mouth is open, surface waters move through the estuary quickly when the mouth is open (residence times ~ 1day). Similarly mixed waters are rapidly removed from the estuary through the action of tides. However, as tidal action weakens due to a reduction in mouth conveyance, mid-depth and near-bottom saline waters become resident in a stratified estuary. Residence time typically exceeds the period in which muted tides are observed and the mouth closes with these waters still retained in the estuary – thus residence time becomes closure time (over a month in September-October 2009). As stratification develops later in the inner estuary during closure, saline waters are only trapped there later and residence in this location is shorter (still long enough for de-oxygenation) – but these saline waters were already resident in the estuary and have only shifted location. Meanwhile, surface waters will continue to move through and out of the estuary as long as the bed of the mouth channel (or the crest of the berm) is below the estuary water level. This “overflow” state has been observed at the mouth of the Russian River, but this is not common, nor does it persist for more than a few days (PWA, 2010). Even when closed, water is lost through the sand barrier (up to a rate of about 60cfs later in the September 2009 closure). These waters are primarily lost from above the pycnocline (Section 3.4.2), implying a residence time for near-surface waters of order 10 days (calculated from volume/seepage rate). While this weak throughflow entrains some water from the upper pycnocline, water beneath the pycnocline is

unaffected and remains resident for at least a month (the period of closure). Indeed, some deeper waters remain trapped and resident for days after the 5 October breaching.

Water column conditions and thus habitat value in the closed estuary are largely controlled by stratification. This study has identified several key factors:

- The importance of processes controlling the amount of salt contained in the estuary at the time of closure – and thus the subtle importance of exactly how and when the mouth closes relative to high-low and spring-neap tidal cycles and river flow variation.
- The importance of periods when the mouth is semi-closed, allowing outflow but precluding significant inflow of new seawater. The outflowing surface water removes intermediate density water from above the central pycnocline, thus sharpening the vertical density gradient and increasing vertical stability.
- The importance of wave overwash events at the time of closure or after closure as they inject undiluted seawater into the estuary with no subsequent outflow. These events increase the total mass of salt and the overall stability of the stratification.
- The importance of the diurnal sea breeze in generating a seiche in the estuary with currents strong enough to slowly mix salt vertically and re-distribute it horizontally (including possible control of intrusion of saline waters into the inner estuary). In addition, the surface wind stress may have a direct impact on mixing near the mouth.
- The importance of small variations in river water through-flow and water depths in precluding or allowing intrusion of saline waters over shoals in the inner estuary.
- The importance of light and thermal radiation that penetrates into the stable pycnocline, resulting in increased dissolved oxygen and increased temperature in mid-depth layers that are precluded from mixing with either deeper or shallower waters in the estuary.

The data described here and in the companion data report (Behrens & Largier 2010) provide a clear view of circulation and stratification in the Russian River estuary during a low-flow summer/fall. Future work should be directed at two suites of questions – those relating to how stratification during closure relates to the extent and value of water column habitat for juvenile steelhead (as posed by NMFS 2008), and those relating to the processes that control stratification and mixing in the estuary (with a view to understanding how humans do or can influence the outcome). Specifically, the following topics are of primary concern:

1. Juvenile salmon habitat. Based on known affinity for given salinity, temperature and dissolved oxygen values, our knowledge of the distribution of these parameters may be converted to quantitative knowledge of the spatial extent of primary, marginal and undesirable water column habitat. Improvements to existing information would come

from data collection in shallow-water littoral zones (particularly those inundated at higher water levels) and from measurement of turbulent velocities in the main channel and littoral zones. In addition to quantifying salmon habitat, it may be possible to quantify the extent of habitat for primary invertebrate prey, which may be impacted by near-bottom hypoxia/anoxia.

2. Dissolved oxygen levels during breaching. High velocities immediately following breaching of the estuary mouth may resuspend large amounts of labile organic matter that can be respired (i.e., biological oxygen demand BOD. A brief but widespread drop in DO has been observed in other estuaries following breaching after long closure periods. Data on BOD prior to, during and immediately after breaching – as well as DO data – would allow assessment of this risk.

3. Stability of water column. The potential energy anomaly and Richardson Number values provide indices of mixing and stability, but these do not allow an assessment of the likelihood of mixing. Repeated high-resolution CTD profiles combined with profiles of turbulent energy at selected places and times are necessary for a process-oriented understanding of mixing rates and the potential for breakdown of stratification over time (which is necessary for re-oxygenation of near-bottom waters).

4. Wind-driven seiche. The seiche appears to be the primary form of kinetic energy in the mid/inner estuary during closure. It is likely that not only horizontal redistribution of density but also net vertical exchange of salinity and density is controlled by this process. Improved data on wind forcing along the estuary and responses in terms of current velocities and transport are needed to properly assess this phenomenon.

5. Seepage loss. The apparent loss of estuarine water through the sand barrier at the mouth is a critical factor in flushing the surface layer, but it also may play a key role in destabilizing the stratification near the mouth as a result of even small losses of high salinity water from beneath the pycnocline. Our knowledge can be improved through better knowledge of surface water inflows and surface-groundwater exchange (improving the mass-balance approach) and/or through direct study of the rate, depth and salinity of flows through the berm.

6. Non-conventional overflows. Wave overwash and surface overflow have been little studied in estuaries, but it is clear that these peculiar flows play a key role in governing stratification and both are closely related to the height of saddle points in the berm crest. Advances can be made through improved observations of these processes, as well as improved observation and understanding of processes controlling berm morphology.

5. Literature Reviewed

Battalio, B., D. Danmeier, and P. Williams, 2006. Predicting closure and breaching frequencies of small tidal inlets – a quantified conceptual model. *Proceedings of the 30th Conference on Coastal Engineering*, San Diego, CA, USA.

Behrens, D., F. Bombardelli, J. Largier, and E. Twohy (2009). Characterization of time and spatial scales of a migrating rivermouth. *Geophysical Research Letters* 36, L02806 doi: 10.1029/2008GL036350.

Behrens, D.K. and J.L. Largier, 2010. *Preliminary Study of Russian River Estuary: Circulation and Water Quality Monitoring – 2009 Data Report*. Report to Sonoma County Water Agency prepared by Bodega Marine Laboratory (UC Davis), 72pp.

Bodega Ocean Observing Node (BOON), 2010. Selected atmospheric data. Retrieved from: http://www.bml.ucdavis.edu/boon/data_access.html

Dean, R. G., and R. A. Dalrymple, 2002. *Coastal Processes; with Engineering Applications*, 488 pp., Cambridge Univ. Press, New York.

Dennison, W. R. Orth, K. Moore, J. Stevenson, V. Carter, S. Kollar, P. Bergstrom, and R. Batiuk, 1993. Assessing water quality with submersed aquatic vegetation: Habitat requirements as barometers of Chesapeake Bay health. *BioScience* 43(2): 86-94.

Donnelly, C., N. Kraus, and M. Larson, 2006. State of knowledge on measurement and modeling of coastal overwash. *Journal of Coastal Research* 22(4): 965-991.

EDS, 2009. Unpublished sidescan sonar bathymetry data and LiDAR topography data for the Russian River from the mouth to Duncan Mills. Environmental Data Solutions, conducted for Sonoma County Water Agency.

Fischer, H., J. List, R. Koh, J. Imberger, and N. Brooks, 1979. *Mixing in Inland and Coastal Waters.* London: Academic Press.

Friedrichs, C., L. Wright, D. Hepworth, and S. Kim, 2000. Bottom-boundary-layer processes associated with fine sediment accumulation in coastal seas and bays. *Continental Shelf Research* 20: 807-841.

Gladstone, W., N. Hacking, and V. Owen, 2006. Effects of artificial openings of intermittently opening estuaries on macroinvertebrate assemblages of the entrance barrier. *Estuarine, Coastal and Shelf Science* 67, 708-720.

Goodwin, P. and K. Cuffe, 1994. *Russian River Estuary Study: Hydrologic Aspects of an Estuary Management Plan*. Technical report for Sonoma Co. Dept. of Planning, 194 pp., Philip Williams and Assoc., San Francisco, Calif.

Komar, P.D., 1997. *Beach Processes and Sedimentation*. Prentice-Hall, New Jersey.

Kraus, N., S. Munger, and K. Patsch, 2008. Barrier beach breaching from the lagoon side, with reference to Northern California, *Shore and Beach*, 76, 33-43.

Largier, J. L. and S. Taljaard, 1991. The dynamics of tidal intrusion, retention and removal of seawater in a bar-built estuary. *Estuarine, Coastal and Shelf Science*, 33, 325-338.

Largier, J. L. and J. H. Slinger, 1991. Circulation in highly stratified southern African estuaries. *South African Journal of Aquatic Science*, 17(1/2), 103-115.

Largier, J.L., B.A. Magnell and C.D. Winant, 1993. Subtidal circulation over the northern California shelf. *Journal of Geophysical Research*, 98(C10), 18147-18179.

Monismith, S. 2010. Mixing in estuaries. In Valle-Levinson (Ed.), *Contemporary Issues in Estuarine Physics* (pp. 145-185). New York, NY: Cambridge University Press.

NMFS, 2008. *Biological Opinion for Water Supply, Flood Control Operations, and Channel Maintenance conducted by the U.S. Army Corps of Engineers, the Sonoma County Water Agency, and the Mendocino County Russian River Flood Control and Water Conservation Improvement District in the Russian River Watershed*. National Marine Fisheries Service, Southwest Region, Reference F/SWR/2006/07316.

O'Callahan, J., C.Pattiaratchi, and D. Hamilton, 2007. The response of circulation and salinity in a micro-tidal estuary to subtidal oscillations in coastal sea surface elevation. *Continental Shelf Research* 27, 1947-1965.

O'Donahue, M. and W. Dennison, 1997. Phytoplankton productivity response to nutrient concentrations, light availability and temperature along an Australian estuarine gradient. *Estuaries* 20(3): 521-533.

Penman, H. 1948. Natural evaporation from open water, bare soil and grass. *Proceedings of the Royal Society, London*, Series A, 193: 120-145.

PWA, 2010. *Russian River Estuary Outlet Channel Adaptive Management Plan 2010*. Philip Williams and Associates, San Francisco, CA, 102pp.

Rice, M. P. 1974. Closure conditions: mouth of the Russian River, *Shore and Beach,* 42, 15-20.

Simpson, J. and D. Bowers, 1981. Models of stratification and frontal movement in shelf seas. *Deep-Sea Research* 28 (7), 727-738.

Simpson, J., J. Brown, J. Matthews, and G. Allen, 1990. Tidal straining, density currents, and stirring in the control of estuarine stratification. *Estuaries* 13(2): 125-132.

Simpson, J., E. Williams, L. Brasseur, and J. Brubaker, 2005. The impact of tidal straining on the cycle of turbulence in a partially stratified estuary. *Continental Shelf Research* 25: 51-64.

Tamminga, A.D. and J.L. Largier, 2009. *Depletion of Dissolved Oxygen in a Stratified Closed Estuary: Russian River, California*. Bodega Marine Laboratory, 32pp.

UNESCO, 1981. Tenth report of the joint panel on oceanographic tables and standards (UNESCO technical papers in marine science, no. 36). Retrieved from: http://unesdoc.unesco.org/images/0004/000461/046148eb.pdf